Journal of Quantitative Spectroscopy & Radiative Transfer 113 (2012) 2023–2039

Contents lists available at SciVerse ScienceDirect

Journal of Quantitative Spectroscopy & Radiative Transfer

journal homepage: www.elsevier.com/locate/jqsrt

Model for land surface reflectance treatment: Physical derivation, application for bare soil and evaluation on airborne and satellite measurements

Pavel Litvinov [a,*], Otto Hasekamp [b], Oleg Dubovik [a], Brian Cairns [c]

[a] Laboratoire d'Optique Atmosphérique, CNRS Universite de Lille 1, Bat P5 Cite scientifique, 59655 Villeneuve d'Ascq, France
[b] SRON Netherlands Institute for Space Research, Sorbonnelaan 2, 3584 CA Utrecht, The Netherlands
[c] NASA Goddard Institute for Space Studies, 2880 Broadway, New York, NY 10025, USA

ARTICLE INFO

Article history:
Received 8 May 2012
Received in revised form
27 June 2012
Accepted 29 June 2012
Available online 7 July 2012

Keywords:
Satellite remote sensing
Surface bidirectional reflectance
Surface polarized reflectance
Surface reflection models
Aerosol properties retrieval

ABSTRACT

For land surfaces and atmospheric aerosol characterization on the basis of satellite and airborne measurements models for surface reflection description are required. At present time for visible and infrared spectral regions semi-empirical model for surface reflection are usually used for these purposes. Due to the lack of physical basis, these models introduce a lot of uncertainties into the problem of aerosol and surface properties retrieval. In this paper we consider the possibility of using physically based models for bidirectional reflection matrix (BRM) which can be applied to the problem of simultaneous retrieval of aerosol and land surface properties. The physical model for the BRM is derived from the general solution of the electromagnetic scattering problems by random media. The equation for the reflection matrix is obtained within the far-field approximation when the ladder scattering diagrams are taken into account. To perform analytical averaging over orientation of the surface elements we assume that at different scales the surface can be considered as the Gaussian surface. We use multi-angle photopolarimetric airborne measurements of the Research Scanning Polarimeter (RSP) and satellite POLDER (Polarization and Directionality of the Earth's Reflectances) measurements to investigate the performance of the presented BRM model. The results of the comparison are discussed.

© 2012 Elsevier Ltd. All rights reserved.

1. Introduction

Earth surfaces are important component of the climate system. Their interaction with incoming solar radiation as well as radiative interaction with atmosphere greatly impact on Earth energy budget. Intrinsic reflectance properties of surfaces are described by the bidirectional reflection matrix **R** (BRM), which provides a relation between the Stokes parameters of scattered and incident radiation. On the basis of knowledge of the BRM the surface properties can be retrieved from the remote sensing measurements [1–3]. Moreover, accurate models of BRM at visible and infrared wavelengths are required for retrieval of aerosols properties over Earth surfaces [4–9]. Over the ocean the surface contribution is relatively small and can for most scenes be modeled with sufficient accuracy using physically based model of BRM for water surfaces [4–8]. Over land the surface reflection contribution is, in general, much larger, and shows large spatial variability, representing one of the most important problems for aerosol retrieval algorithms. To describe separately the surface contribution into intensity and polarization characteristics of scattered radiation, the bidirectional reflection distribution function

* Corresponding author.
E-mail addresses: PVLitvinov@mail.ru, Pavel.Litvinov@univ-lille1.fr (P. Litvinov).

0022-4073/$ - see front matter © 2012 Elsevier Ltd. All rights reserved.
http://dx.doi.org/10.1016/j.jqsrt.2012.06.027

(BRDF) and bidirectional polarization distribution function (BPDF) are often used [10–18]. For land surfaces albedo characterization from the satellite data as well as for aerosol properties retrieval over land the semi-empirical models of BRDF and BPDF are usually applied [10–18]. Because of the lack of physical basis, the parameters of the semi-empirical BRDF models are not necessarily consistent with the parameters of the semi-empirical BPDF models. Moreover they are slightly related or not related at all to the actual physical parameters of the scattering surfaces. That complicates land surface properties characterization and introduces a lot of uncertainties into the problem of aerosol properties retrieval over land [19,20].

Natural Earth land surfaces can be very complex scattering objects which differ by their physical, optical, geometrical, statistical, etc. properties. The physical description of scattering by such media can be quite complicated. Moreover, there can not be one universal physically based BRM model which could be applied to all possible types of surfaces. Nevertheless, very often the type of a surface can be known or easily established (for example, bare soil, desert, vegetated surfaces, etc.). In this case the usage of physically based models of BRM for aerosol retrieval over land can gain an advantage over the semi-empirical ones. Moreover the physical models of BRM are very important on their own for surface characterisation. At present time, on the one hand, there are space borne and airborne instruments which provide multi-spectral, multi-angle photopolarimetric measurements over big variety of land surfaces which can be used in evaluation of the physical models of BRM for land surfaces [21–28]. On the other hand, big progress is now achieved in the theory of light scattering by random media. It is not utilized in the existent BRDF and BPDF models for the visible and infrared spectral regions (see, for example, [1,3,29–34]). In general, most of these approaches are very complicated or time consuming to be used in the retrieval schemes (for example, for aerosol retrieval over land). They can be used as a start point for obtaining simplified BRM models. In this paper we follow this way to develop simplified but still physical models for the reflection matrix **R** which can be used for simultaneous retrieval of aerosol and land surface properties.

Physical derivation of BRM we start from the general solution of the electromagnetic scattering problems by random media [3,34]. The equation for the reflection matrix **R** is obtained within the far-field approximation when the ladder scattering diagrams are taken into account. Also, to perform analytical averaging over orientation of surface elements we assume that at different scales the surface can be considered as Gaussian surface. In general, we present the reflection matrix as a sum of three other matrices: the first one describes Fresnel part of the scattered radiation, the second one describes diffuse radiation emerging from single surface element, and the third matrix takes into account multiple scattering between different surface elements. In the presented model the BRDF and BPDF are related to the elements of the reflection matrix **R**. The model applies strong constraints on the spectral dependence of the model parameters and relates the BRDF and BPDF model parameters to each other.

We use multi-angle photopolarimetric airborne measurements of the Research Scanning Polarimeter (RSP) [25–27] and satellite POLDER (Polarization and Directionality of the Earth's Reflectances) measurements [21,22] to investigate the performance of the derived BRM model in terms of the three aspects for BRDF and BPDF models [19,20] which are important for aerosol properties retrieval over land: (i) there must be known constraints on and invariances of the spectral and angular dependences of the BRDF and BPDF; (ii) BRDF and BPDF models should be able to describe correctly the surface signal with the geometry of the measurements (flexibility), as well as (iii) for all other geometries (predictability).

The paper is organized as follows: in the section "General formulas and definitions" we start from the general solution of Helmholtz inhomogeneous equation and obtain the equation for the reflection matrix from random rough medium. The equations obtained in this section are not averaged over ensemble of scattering elements, and thus they are not related to any type of surfaces. In the section "Physical model of BRM (BRDF and BPDF)" we perform the averaging over ensemble of scattering elements and introduce simplified description for the matrices describing the diffuse radiation emerging from single surface element and the multiple scattering between different surface elements. Here averaging and assumption are mainly applicable for bare soil and desert surfaces. In the section "Fitting to RSP and POLDER BRDF/BPDF measurements" we evaluate the presented model on some RSP and POLDER measurements for bare soil and desert surfaces. The section "Conclusions and Discussion"

Table 1
Definition of the main symbols.

$\mathbf{E}$	Strength of the electric field
$\overleftrightarrow{G}_0$	Free space dyadic Green's function
$\overleftrightarrow{T}$	Dyadic transition operator
$\overleftrightarrow{U}$	Scattering potential
$\overleftrightarrow{A}$	Amplitude scattering dyad
$\mathbf{S}$	Amplitude scattering matrix
$\mathbf{Z}$	Phase matrix
$\mathbf{R}$	Reflection matrix
$\mathbf{R}^{1Fr}$	Fresnel part of the reflection matrix
$\mathbf{R}^{1diff}$	Diffuse part of the reflection matrix
$\mathbf{R}^{mult}$	Reflection matrix for multiple scattering part
$\mathbf{I}$	Stokes vector
f_{pdf}	Probability density function
f_{shad}	Shadowing function due to rough surface hight distribution
f_{shad}^{orien}	Shadowing function due to orientation of surface elements
m	Complex refractive index of the medium
k	Wavenumber
λ	Wavelength
l_{ch}	Characteristic length
l_{ext}	Extinction length
l_{cor}	Correlation length
μ	Cosine of zenith angle (in the local or reference coordinate system)
α, β	Angles of rotation from one coordinate system to another
a_{iso}	Albedo of the surface element
σ^2	Mean square surface slope
b_{iso}	Parameter for multiple scattering
δ_{Fr}	Fraction of surface providing Fresnel reflection
Δ_p	Parameter for polarization

contains brief summarizing the main results of the paper, the discussion of weak and strong points of the presented model and the applied approach as well as the possibilities for model improvement. The definition of the main symbols of the paper is presented in Table 1.

2. General formulas and definitions

Let us consider measurement provided with an optical instrument with acceptance solid angle $\Delta\Omega_{obs}$ and situated at a distance r from a scattering object (see Fig. 1). Optical instruments measure the Stokes parameters of radiation. Nevertheless, let us start from the general consideration of the electromagnetic scattering by a medium, surrounded by an infinite, homogeneous, linear, isotropic, nonmagnetic and nonabsorbing space. The electric field accepted by the instrument can be determined from the volume integral equation, which is the solution of the inhomogeneous Helmholtz equation (see, for example, [1,3,34,35]):

$$\mathbf{E}(\mathbf{r}) = \mathbf{E}_{inc}(\mathbf{r}) + \int_{V_{obs}} \int_V \overleftrightarrow{G}_0(\mathbf{r},\mathbf{r}')\overleftrightarrow{T}(\mathbf{r}',\mathbf{r}'')\mathbf{E}_{inc}(\mathbf{r}'')d^3\mathbf{r}'d^3\mathbf{r}''. \quad (1)$$

Here V_{obs} is the scattering volume restricted by the surface ΔS_{obs} observed from the instrument, V is the whole volume of scattering medium (see Fig. 1), $\overleftrightarrow{G}_0(\mathbf{r},\mathbf{r}')$ is the free space dyadic Green's function, $\overleftrightarrow{T}(\mathbf{r}',\mathbf{r}'')$ is the dyadic transition operator [3,34–36], $\mathbf{E}_{inc}(\mathbf{r}'')$ is the incident electric field:

$$\overleftrightarrow{G}_0(\mathbf{r},\mathbf{r}') = \left(\overleftrightarrow{I} + \frac{\nabla_{\mathbf{r}} \otimes \nabla_{\mathbf{r}}}{k^2}\right)\frac{\exp(ik|\mathbf{r}-\mathbf{r}'|)}{4\pi|\mathbf{r}-\mathbf{r}'|}, \quad (2)$$

$$\overleftrightarrow{T}(\mathbf{r}',\mathbf{r}'') = \overleftrightarrow{U}(\mathbf{r}')\delta(\mathbf{r}'-\mathbf{r}'') + \overleftrightarrow{U}(\mathbf{r}')\int_V \overleftrightarrow{G}_0(\mathbf{r}',\mathbf{r}''')\overleftrightarrow{T}(\mathbf{r}''',\mathbf{r}'')d^3\mathbf{r}''', \quad (3)$$

$$\overleftrightarrow{U}(\mathbf{r}') = \begin{cases} 0, & \mathbf{r}' \notin V, \\ k^2(m^2-1), & \mathbf{r}' \in V. \end{cases} \quad (4)$$

$$\mathbf{E}_{inc} = \overleftrightarrow{G}_0(\mathbf{r}'',\mathbf{r}_0)\mathbf{J}_0(\mathbf{r}_0). \quad (5)$$

Here $\overleftrightarrow{U}(\mathbf{r}')$ is the scattering potential [3,34–36], $m(\mathbf{r})$ is the complex refractive index of the medium relative to that of the surrounding space, $k = 2\pi/\lambda$ is the wavenumber in surrounding space (λ is the wavelength), $\mathbf{J}_0$ is a source of radiation (we assume that the source of radiation is situated in the far-field zone from the observed scattering volume V_{obs}).

Eq. (1) can be applied both for discrete and continuous media [3,34–38]. For the continuous media it takes into account surface roughness of the media. For discrete media it takes into account the scatterers distribution both in the volume of the scattering medium and on the surface of the medium. Eq. (1) requires further consideration to be used in practice for scattering signal calculation. For the case of media characterized by constant complex reflective index m, the integral over the volume in Eq. (1) can be transferred to the integral over surface. Then the well developed approaches for the continuous media with random rough surfaces can be used to describe the scattered field [1,3]. For the discrete random media the problem is more complicated, since it is necessary to take into account the near-field effects, different kinds of scatterers properties correlation in the medium, the scatterers distribution in the volume and on the surface, etc. [3,31–33]. In this paper we consider the random media (both discrete and continuous) with rough surfaces.

Let us subdivide the volume V_{obs} on the smaller volume elements V_i, restricted by the surfaces ΔS_i (see Fig. 2). For each volume element V_i the transition operator $\overleftrightarrow{T}_i(\mathbf{r}_i',\mathbf{r}_i'')$ can be introduced similar to that given by Eq. (3) [36–38]:

$$\overleftrightarrow{T}_i(\mathbf{r}_i',\mathbf{r}_i'') = \overleftrightarrow{U}(\mathbf{r}_i')\delta(\mathbf{r}_i'-\mathbf{r}_i'') + \overleftrightarrow{U}(\mathbf{r}_i')\int_{V_i} \overleftrightarrow{G}_0(\mathbf{r}_i',\mathbf{r}_i''')\overleftrightarrow{T}_i(\mathbf{r}_i''',\mathbf{r}_i'')d^3\mathbf{r}_i'''. \quad (6)$$

Let us assume now that measurement is performed at the distance r (see Fig. 1) which is much bigger than the wavelength λ of the incident radiation and the characteristic length l_{obs}^{ch} of the observed volume V_{obs} ($l_{obs}^{ch} \sim \sqrt[3]{V_{obs}}$):

$$kr \gg 1, \quad r \gg l_{obs}^{ch}. \quad (7)$$

Also, we assume that the instrument is situated in the far-field zone from each scattering volume elements V_i and the characteristic lengths l_i^{ch} of the volume elements ($l_i^{ch} \sim \sqrt[3]{V_i}$) are much bigger than λ:

$$kr_i \gg 1, \quad r_i \gg l_i^{ch}, \quad l_i^{ch} \ll \sqrt{\lambda r}, \quad l_i^{ch} \gg \lambda. \quad (8)$$

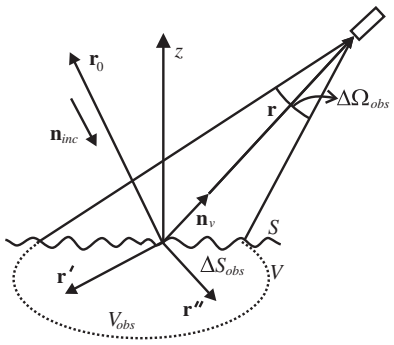

Fig. 1. Schematic representation of the electromagnetic scattering problem.

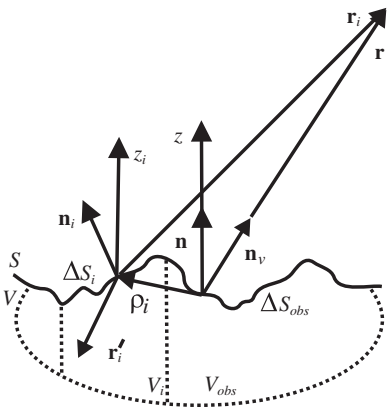

Fig. 2. Schematic representation of subdivision of surface.

Then, for the field accepted by the instrument, one can write as follows [35–37]:

$$\mathbf{E}(\mathbf{r}) = \mathbf{E}_{inc}(\mathbf{r}) + \sum_{ij} \overleftrightarrow{G}_0(\mathbf{r},\boldsymbol{\rho}_i) \times \int_{V_i}\int_{V_j} \exp(-ik\hat{\mathbf{r}}_i\mathbf{r}_i') \overleftrightarrow{T}_{ij}(\boldsymbol{\rho}_i+\mathbf{r}_i',\boldsymbol{\rho}_j+\mathbf{r}_j'') \times \exp(-ik\hat{\mathbf{r}}_{0j}\mathbf{r}_j'') d^3\mathbf{r}_i' d^3\mathbf{r}_j'' \overleftrightarrow{G}_0(\boldsymbol{\rho}_j,\mathbf{r}_0)\mathbf{J}_0, \quad (9)$$

where the vectors $\boldsymbol{\rho}_i$ and $\mathbf{r}_i'$ are related to the vector $\mathbf{r}'$: $\mathbf{r}' = \boldsymbol{\rho}_i + \mathbf{r}_i'$ (similarly, $\mathbf{r}'' = \boldsymbol{\rho}_j + \mathbf{r}_j''$), and the vectors $\boldsymbol{\rho}_i$ and $\mathbf{r}_i$ are related to the vector $\mathbf{r}$: $\mathbf{r} = \boldsymbol{\rho}_i + \mathbf{r}_i$ (similarly, $\mathbf{r}_0 = \boldsymbol{\rho}_j + \mathbf{r}_{0j}$) (Fig. 2). The transition operator $\overleftrightarrow{T}_{ij}(\boldsymbol{\rho}_i+\mathbf{r}_i',\boldsymbol{\rho}_j+\mathbf{r}_j'')$ describes single scattering by the different volume elements V_i as well as multiple scattering between the elements. It can be written as follows [36,37]:

$$\overleftrightarrow{T}_{ij}(\boldsymbol{\rho}_i+\mathbf{r}_i',\boldsymbol{\rho}_j+\mathbf{r}_j'') = \overleftrightarrow{T}_i(\boldsymbol{\rho}_i+\mathbf{r}_i',\boldsymbol{\rho}_i+\mathbf{r}_i'')\delta_{ij} + \int_{V_i}\int_{V_j} \overleftrightarrow{T}_i(\boldsymbol{\rho}_i+\mathbf{r}_i',\boldsymbol{\rho}_i+\mathbf{r}_i''') \overleftrightarrow{G}(\boldsymbol{\rho}_i+\mathbf{r}_i''',\boldsymbol{\rho}_j+\mathbf{r}_j^{(4)}) \times \overleftrightarrow{T}_j(\boldsymbol{\rho}_j+\mathbf{r}_j^{(4)},\boldsymbol{\rho}_j+\mathbf{r}_j'') d^3\mathbf{r}_i''' d^3\mathbf{r}_j^{(4)}. \quad (10)$$

The Green's function $\overleftrightarrow{G}(\boldsymbol{\rho}_i+\mathbf{r}_i''',\boldsymbol{\rho}_j+\mathbf{r}_j^{(4)})$ in Eq. (10) describes propagation and scattering of waves on the way from the volume element V_j to the volume elements V_i [36,37]:

$$\overleftrightarrow{G}(\boldsymbol{\rho}_i+\mathbf{r}_i''',\boldsymbol{\rho}_j+\mathbf{r}_j^{(4)}) = \overleftrightarrow{G}_0(\boldsymbol{\rho}_i+\mathbf{r}_i''',\boldsymbol{\rho}_j+\mathbf{r}_j^{(4)})(1-\delta_{ij}) + \sum_{k\neq i}\sum_{k_1\neq j}\int_{V_k}\int_{V_{k_1}} \overleftrightarrow{G}_0(\boldsymbol{\rho}_i+\mathbf{r}_i''',\boldsymbol{\rho}_k+\mathbf{r}_k''') \overleftrightarrow{T}_{kk_1}(\boldsymbol{\rho}_k+\mathbf{r}_k''',\boldsymbol{\rho}_{k_1}+\mathbf{r}_{k_1}^{(4)}) \times \overleftrightarrow{G}_0(\boldsymbol{\rho}_{k_1}+\mathbf{r}_{k_1}^{(4)},\boldsymbol{\rho}_j+\mathbf{r}_j^{(4)}) d^3\mathbf{r}_k''' d^3\mathbf{r}_{k_1}^{(4)}. \quad (11)$$

In Eq. (9) the Green's functions $\overleftrightarrow{G}_0(\mathbf{r},\boldsymbol{\rho}_i)$ and $\overleftrightarrow{G}_0(\boldsymbol{\rho}_j,\mathbf{r}_0)$ describe propagation of waves in the free space (without any scattering) from the surface of medium to the detector and from the source of radiation to the surface. Because of the rough surface of the medium (because of scatterers distribution on the surface) scattering and absorption is possible also on these paths. To take these absorption and scattering into account the averaged Green's function $\langle \overleftrightarrow{G}_0(\mathbf{r},\boldsymbol{\rho}_i)\rangle$ and $\langle \overleftrightarrow{G}_0(\boldsymbol{\rho}_j,\mathbf{r}_0)\rangle$ can be introduced in Eq. (9) instead of the Green's functions $\overleftrightarrow{G}_0(\mathbf{r},\boldsymbol{\rho}_i)$ and $\overleftrightarrow{G}_0(\boldsymbol{\rho}_j,\mathbf{r}_0)$:

$$\mathbf{E}(\mathbf{r}) = \mathbf{E}_{inc}(\mathbf{r}) + \sum_{ij} \langle \overleftrightarrow{G}_0(\mathbf{r},\boldsymbol{\rho}_i)\rangle \int_{V_i}\int_{V_j} \exp(-ik\hat{\mathbf{r}}_i\mathbf{r}_i') \times \overleftrightarrow{T}_{ij}(\boldsymbol{\rho}_i+\mathbf{r}_i',\boldsymbol{\rho}_j+\mathbf{r}_j'') \exp(-ik\hat{\mathbf{r}}_{0j}\mathbf{r}_j'') d^3\mathbf{r}_i' d^3\mathbf{r}_j'' \langle \overleftrightarrow{G}_0(\boldsymbol{\rho}_j,\mathbf{r}_0)\rangle \mathbf{J}_0, \quad (12)$$

$$\langle \overleftrightarrow{G}_0(\mathbf{r},\boldsymbol{\rho})\rangle = \overleftrightarrow{G}_0(\mathbf{r},\boldsymbol{\rho}) f_{ext}(\boldsymbol{\rho},\mathbf{r}-\boldsymbol{\rho}), \quad (13)$$

where $f_{ext}(\boldsymbol{\rho},\mathbf{r}-\boldsymbol{\rho})$ is the function which describes extinction of the wave while it is leaving the surface or incident on the surface. It depends on the direction of the wave propagation. For a flat surface it is equal to 1. Here we consider statistically isotropic medium, thus, the extinction is the same for different states of the wave polarization and can be described by scalar function. Since $r \gg l_{obs}^{ch}$ and $r_0 \gg l_{obs}^{ch}$ ($r \gg \rho_i$ and $r_0 \gg \rho_j$) then the asymptotic Green's function can be used (see [3,34,35], Eqs. (79)–(83) in Appendix A). Then Eq. (12) can be written in the following form:

$$\mathbf{E}(\mathbf{r}) = \mathbf{E}_{inc}(\mathbf{r}) + (\overleftrightarrow{I} - \hat{\mathbf{r}}\otimes\hat{\mathbf{r}}) \times \sum_{ij} \frac{\exp(ikr_i)}{r} f_{ext}(\boldsymbol{\rho}_i,\mathbf{r}-\boldsymbol{\rho}_i) \overleftrightarrow{A}_{ij}(\boldsymbol{\rho}_i,\boldsymbol{\rho}_j;\hat{\mathbf{r}}_i,-\hat{\mathbf{r}}_{0j}) \times \frac{\exp(kr_j)}{4\pi r_j} f_{ext}(\boldsymbol{\rho}_j,\mathbf{r}_0-\boldsymbol{\rho}_j) \times (\overleftrightarrow{I} - \hat{\mathbf{r}}_0\otimes\hat{\mathbf{r}}_0)\mathbf{J}_0, \quad (14)$$

where $\overleftrightarrow{A}_{ij}$ is the amplitude scattering dyad:

$$\overleftrightarrow{A}_{ij}(\boldsymbol{\rho}_i,\boldsymbol{\rho}_j;\hat{\mathbf{r}}_i,-\hat{\mathbf{r}}_{0j}) = \frac{1}{4\pi}\int_{V_i}\int_{V_j} \exp(-ik\hat{\mathbf{r}}_i\mathbf{r}_i') \overleftrightarrow{T}_{ij}(\boldsymbol{\rho}_i+\mathbf{r}_i',\boldsymbol{\rho}_j+\mathbf{r}_j'') \times \exp(-ik\hat{\mathbf{r}}_{0j}\mathbf{r}_j'') d^3\mathbf{r}_i' d^3\mathbf{r}_j''. \quad (15)$$

To obtain the equation for $\overleftrightarrow{A}_{ij}$ let us consider Eqs. (10) and (11) and assume that the characteristic length of each volume element is much bigger than the extinction length in the medium l_{ext}:

$$l_i^{ch} \gg l_{ext}. \quad (16)$$

The determination of the extinction length for densely packed medium of the wavelength-sized scatterers may be a non-trivial problem [31,39,40] and is not the topic of this paper. Here, making the assumption (16), we neglect volume multiple scattering between different elements V_i and keep in Eqs. (10) and (11) only the multiple scattering between surfaces ΔS_i restricting the volume elements V_i. Also, to separate variables in the Green's functions describing propagation from one surface element ΔS_i to another ΔS_j we assume that both elements are situated in the far-field zone of each other (see Eq. (84) in Appendix B). This assumption is not always true, especially when adjacent surface elements are considered. Nevertheless, even in this situation the far-field approximation can still provide satisfactory result if the single scattering from an isolated surface element gives the main contribution into the scattered signal or when the angular dependence of scattered radiation is slightly changed within the solid angle at which the one macroscopic scattering element is visible from another one. Then from Eqs. (10), (11) and (15) one can obtain the equation for $\overleftrightarrow{A}_{ij}$ written as order of scattering expansion:

$$\overleftrightarrow{A}_{ij}(\boldsymbol{\rho}_i,\boldsymbol{\rho}_j;\hat{\mathbf{r}}_i,-\hat{\mathbf{r}}_{0j}) = \overleftrightarrow{A}_i(\boldsymbol{\rho}_i;\hat{\mathbf{r}}_i,-\hat{\mathbf{r}}_{0i})\delta_{ij} + \overleftrightarrow{A}_i(\boldsymbol{\rho}_i;\hat{\mathbf{r}}_i,\hat{\mathbf{r}}_{ji})(\overleftrightarrow{I} - \hat{\mathbf{r}}_{ji}\otimes\hat{\mathbf{r}}_{ji}) \frac{\exp(ikr_{ji})}{r_{ji}} \times f_{ext}(\boldsymbol{\rho}_i,\boldsymbol{\rho}_j,\mathbf{r}_{ji}) \overleftrightarrow{A}_j(\boldsymbol{\rho}_j;\hat{\mathbf{r}}_{ji},-\hat{\mathbf{r}}_{0j})(1-\delta_{ij}) + \sum_{\substack{k\neq i\\ k\neq j}} \overleftrightarrow{A}_i(\boldsymbol{\rho}_i;\hat{\mathbf{r}}_i,\hat{\mathbf{r}}_{ki})(\overleftrightarrow{I} - \hat{\mathbf{r}}_{ki}\otimes\hat{\mathbf{r}}_{ki}) \times \frac{\exp(ikr_{ki})}{r_{ki}} f_{ext}(\boldsymbol{\rho}_i,\boldsymbol{\rho}_k,\mathbf{r}_{ki}) \overleftrightarrow{A}_k(\boldsymbol{\rho}_k;\hat{\mathbf{r}}_{ki},\hat{\mathbf{r}}_{jk}) \times (\overleftrightarrow{I} - \hat{\mathbf{r}}_{jk}\otimes\hat{\mathbf{r}}_{jk}) \frac{\exp(ikr_{jk})}{r_{jk}} f_{ext}(\boldsymbol{\rho}_k,\boldsymbol{\rho}_j,\mathbf{r}_{jk}) \overleftrightarrow{A}_j(\boldsymbol{\rho}_j;\hat{\mathbf{r}}_{jk},-\hat{\mathbf{r}}_{0j}) + \cdots, \quad (17)$$

where, for example, $\mathbf{r}_{ji} = \boldsymbol{\rho}_i - \boldsymbol{\rho}_j$, f_{ext} is, as previously, the function describing extinction of radiation on the path from one scattering surface element to another. The amplitude scattering dyad for the certain isolated surface volume

element V_i can be defined similar to Eq. (15):

$$\overleftrightarrow{A}_i(\boldsymbol{\rho}_i;\hat{\mathbf{r}}_i,-\hat{\mathbf{r}}_{0i}) = \frac{1}{4\pi}\int_{V_i}\int_{V_i}\exp(-ik\hat{\mathbf{r}}_i\mathbf{r}'_i)\overleftrightarrow{T}_i(\boldsymbol{\rho}_i+\mathbf{r}'_i,\boldsymbol{\rho}_i+\mathbf{r}''_i) \times\exp(-ik\hat{\mathbf{r}}_{0i}\mathbf{r}''_i)d^3\mathbf{r}'_i d^3\mathbf{r}''_i, \tag{18}$$

where $\overleftrightarrow{T}_i(\boldsymbol{\rho}_i+\mathbf{r}'_i,\boldsymbol{\rho}_i+\mathbf{r}''_i)$ is defined by Eq. (6).

From Eq. (17) one can obtain the equation for the amplitude scattering matrix $\mathbf{S}_{ij}$, relating the components of incident and scattered fields defined in the coordinate systems with axes z directed towards the incident and scattered directions $-\hat{\mathbf{r}}_0$ and $\hat{\mathbf{r}}$ (see Appendix B, Eqs. (85)–(88)):

$$\mathbf{E}_{sc}(\mathbf{r}) = \sum_{ij}\frac{\exp(ikr_i)}{r}f_{ext}(\boldsymbol{\rho}_i,\mathbf{r}-\boldsymbol{\rho}_i)\mathbf{S}_{ij}(\boldsymbol{\rho}_i,\boldsymbol{\rho}_j;\hat{\mathbf{r}}_i,-\hat{\mathbf{r}}_{0j}) \times f_{ext}(\boldsymbol{\rho}_j,\mathbf{r}_0-\boldsymbol{\rho}_j)\exp(-ik\hat{\mathbf{r}}_0\boldsymbol{\rho}_j)\mathbf{E}^0_{inc}, \tag{19}$$

where $\mathbf{E}^0_{inc}$ is the amplitude of the incident field:

$$\mathbf{E}^0_{inc} = \frac{\exp(ikr_0)}{4\pi r_0}(\overleftrightarrow{I}-\hat{\mathbf{r}}_0\otimes\hat{\mathbf{r}}_0)\mathbf{J}_0, \tag{20}$$

$$\mathbf{S}_{ij}(\boldsymbol{\rho}_i,\boldsymbol{\rho}_j;\hat{\mathbf{r}}_i,-\hat{\mathbf{r}}_{0j}) = (\overleftrightarrow{I}-\hat{\mathbf{r}}\otimes\hat{\mathbf{r}})\overleftrightarrow{A}_{ij}(\boldsymbol{\rho}_i,\boldsymbol{\rho}_j;\hat{\mathbf{r}}_i,-\hat{\mathbf{r}}_{0j})(\overleftrightarrow{I}-\hat{\mathbf{r}}_0\otimes\hat{\mathbf{r}}_0), \tag{21}$$

$$\begin{aligned}\mathbf{S}_{ij}(\boldsymbol{\rho}_i,\boldsymbol{\rho}_j;\hat{\mathbf{r}}_i,-\hat{\mathbf{r}}_{0j}) &= \mathbf{S}_i(\boldsymbol{\rho}_i;\hat{\mathbf{r}}_i,-\hat{\mathbf{r}}_{0i})\delta_{ij}\\ &+\mathbf{S}_i(\boldsymbol{\rho}_i;\hat{\mathbf{r}}_i,\hat{\mathbf{r}}_{ji})\frac{\exp(ikr_{ji})}{r_{ji}}f_{ext}(\boldsymbol{\rho}_i,\boldsymbol{\rho}_j,\mathbf{r}_{ji})\mathbf{S}_j(\boldsymbol{\rho}_j;\hat{\mathbf{r}}_{ji},-\hat{\mathbf{r}}_{0j})(1-\delta_{ij})\\ &+\sum_{\substack{k\neq i\\ k\neq j}}\mathbf{S}_i(\boldsymbol{\rho}_i;\hat{\mathbf{r}}_i,\hat{\mathbf{r}}_{ki})\frac{\exp(ikr_{ki})}{r_{ki}}f_{ext}(\boldsymbol{\rho}_i,\boldsymbol{\rho}_k,\mathbf{r}_{ki})\mathbf{S}_k(\boldsymbol{\rho}_k;\hat{\mathbf{r}}_{ki},\hat{\mathbf{r}}_{jk})\\ &\times\frac{\exp(ikr_{jk})}{r_{jk}}f_{ext}(\boldsymbol{\rho}_k,\boldsymbol{\rho}_j,\mathbf{r}_{jk})\mathbf{S}_j(\boldsymbol{\rho}_j;\hat{\mathbf{r}}_{jk},-\hat{\mathbf{r}}_{0j})+\cdots,\end{aligned} \tag{22}$$

$$\mathbf{S}_i(\boldsymbol{\rho}_i;\hat{\mathbf{r}}_i,-\hat{\mathbf{r}}_{0i}) = (\overleftrightarrow{I}-\hat{\mathbf{r}}\otimes\hat{\mathbf{r}})\overleftrightarrow{A}_i(\boldsymbol{\rho}_i;\hat{\mathbf{r}}_i,-\hat{\mathbf{r}}_{0i})(\overleftrightarrow{I}-\hat{\mathbf{r}}_0\otimes\hat{\mathbf{r}}_0). \tag{23}$$

In Eqs. (21) and (23) it is assumed that the components of the tensor $(\overleftrightarrow{I}-\hat{\mathbf{r}}\otimes\hat{\mathbf{r}})$ are defined in the coordinate system with axis z' directed along the vector $\hat{\mathbf{r}}$ and with the $x'z'$ plane coincident with meridional plane (see [35], and Eqs. (82), (83), (85)–(88)).

As it was mentioned before, optical instruments measure the Stokes parameters of the radiation which are related to the components of electric field (see, for example, [35] and Eqs. (85)–(90) in Appendix B). Thus, as it follows from Eqs. (89), (19), (22), we have to consider the products of the following sums:

$$E^p_{sc}E^{n*}_{sc} = \left(\sum_{ij}\cdots\right)_{pp'}\left(\sum_{i'j'}\cdots\right)^*_{nn'}E^{p'}_{0inc}E^{n'*}_{0inc}, \tag{24}$$

where E^p, E^n are components of the electric field (see Eq. (85)). Eq. (24) gives different kinds of the scattering diagrams [34]. At the latter stage of the BRM derivation we will have to average Eq. (24) over the positions of each scattering elements. It is well known that if the distance between scatterers much bigger than the wavelength and if it is possible to neglect the correlation of scatterers positions, the ladder and cyclical diagrams will survive after the averaging [34]. The ladder diagrams are described by the radiative transfer equation, whereas the cyclical diagrams contribute to the coherent backscattering effect [29,34,41–45]. In our case, we consider macroscopic surface elements with mutual distances much bigger than the wavelength. It means that the coherent backscattering effect which is due to the constructive interference of waves, multiply scattered by different surface elements, manifests itself in a very narrow angular range in the backscattering direction. Therefore, while considering multiple scattering between different macroscopic surface elements we neglect also the cyclical diagrams and use the ladder scattering approximation. Within the ladder scattering approximation Eq. (24) can be reduced to the following equation:

$$E^p_{sc}E^{n*}_{sc} = \left(\sum_{ij}\cdots\right)_{pp'}\left(\sum_{i'j'}\cdots\right)^*_{nn'}\delta_{ii'}\delta_{jj'}E^{p'}_{0inc}E^{n'*}_{0inc}. \tag{25}$$

Thus, for the Stokes parameters of measured ($\mathbf{I}_{meas}$) and incident ($\mathbf{I}^0_{inc}$) radiation one can write as follows:

$$\mathbf{I}_{meas} = \frac{1}{r^2}\mathbf{Z}(\hat{\mathbf{r}},-\hat{\mathbf{r}}_0)\mathbf{I}^0_{inc}, \tag{26}$$

where

$$\mathbf{Z}(\hat{\mathbf{r}},-\hat{\mathbf{r}}_0) = \sum_{ij}f^2_{ext}(\boldsymbol{\rho}_i,\mathbf{r}-\boldsymbol{\rho}_i)\mathbf{Z}_{ij}(\boldsymbol{\rho}_i,\boldsymbol{\rho}_j;\hat{\mathbf{r}}_i,-\hat{\mathbf{r}}_{0j})f^2_{ext}(\boldsymbol{\rho}_j,\mathbf{r}_0-\boldsymbol{\rho}_j). \tag{27}$$

Here $\mathbf{Z}_{ij}$ is the phase matrix whose elements are related to the elements of $\mathbf{S}_{ij}$ (see [34] and Eqs. (91)–(94) in Appendix B). From Eq. (22) and according to Eq. (25), one can write the equation for $\mathbf{Z}_{ij}$:

$$\begin{aligned}\mathbf{Z}_{ij}(\boldsymbol{\rho}_i,\boldsymbol{\rho}_j;\hat{\mathbf{r}}_i,-\hat{\mathbf{r}}_{0j}) &= \mathbf{Z}_i(\boldsymbol{\rho}_i;\hat{\mathbf{r}}_i,-\hat{\mathbf{r}}_{0i})\delta_{ij}\\ &+\mathbf{Z}_i(\boldsymbol{\rho}_i;\hat{\mathbf{r}}_i,\hat{\mathbf{r}}_{ji})\frac{1}{r^2_{ji}}f^2_{ext}(\boldsymbol{\rho}_i,\boldsymbol{\rho}_j,\mathbf{r}_{ji})\mathbf{Z}_j(\boldsymbol{\rho}_j;\hat{\mathbf{r}}_{ji},-\hat{\mathbf{r}}_{0j})(1-\delta_{ij})\\ &+\sum_{\substack{k\neq i\\ k\neq j}}\mathbf{Z}_i(\boldsymbol{\rho}_i;\hat{\mathbf{r}}_i,\hat{\mathbf{r}}_{ki})\frac{1}{r^2_{ki}}f^2_{ext}(\boldsymbol{\rho}_i,\boldsymbol{\rho}_k,\mathbf{r}_{ki})\mathbf{Z}_k(\boldsymbol{\rho}_k;\hat{\mathbf{r}}_{ki},\hat{\mathbf{r}}_{jk})\\ &\times\frac{1}{r^2_{jk}}f^2_{ext}(\boldsymbol{\rho}_k,\boldsymbol{\rho}_j,\mathbf{r}_{jk})\mathbf{Z}_j(\boldsymbol{\rho}_j;\hat{\mathbf{r}}_{jk},-\hat{\mathbf{r}}_{0j})+\cdots.\end{aligned} \tag{28}$$

For description of the light scattering by random media the reflection matrix $\mathbf{R}$ can be introduced as follows:

$$\mathbf{I}_{meas} = \Delta\Omega_{obs}\mathbf{R}(\hat{\mathbf{r}},-\hat{\mathbf{r}}_0)\mu_0\mathbf{I}^0_{inc}, \tag{29}$$

$$\mathbf{R}(\hat{\mathbf{r}},-\hat{\mathbf{r}}_0) = \frac{\mathbf{Z}(\hat{\mathbf{r}},-\hat{\mathbf{r}}_0)}{\Delta S^{pr}_{obs}\mu_\nu\mu_0}. \tag{30}$$

Here $\Delta\Omega_{obs} = \Delta S^{(pr)}_{obs}\mu_\nu/r^2$, $\Delta S^{(pr)}_{obs}$ is the projection of the observed surface ΔS_{obs} on the average plane with normal $\mathbf{n}$ (see Fig. 2), $\mu_\nu = \mathbf{n}\hat{\mathbf{r}}$, $\mu_0 = \mathbf{n}\hat{\mathbf{r}}_0$.

From Eq. (28) and the definition (30) one can obtain the equations for the reflection matrix $\mathbf{R}$:

$$\mathbf{R}(\hat{\mathbf{r}},-\hat{\mathbf{r}}_0) = \sum_{ij}f^2_{ext}(\boldsymbol{\rho}_i,\mathbf{r}-\boldsymbol{\rho}_i)\frac{\Delta S^{pr}_i}{\Delta S^{pr}_{obs}}\frac{\mathbf{R}_{ij}(\boldsymbol{\rho}_i,\boldsymbol{\rho}_j;\hat{\mathbf{r}}_i,-\hat{\mathbf{r}}_{0j})}{\mu_\nu\mu_0}\mu^{(i)}_\nu\mu^{(j)}_0 \times f^2_{ext}(\boldsymbol{\rho}_j,\mathbf{r}_0-\boldsymbol{\rho}_j), \tag{31}$$

$$\mathbf{R}_{ij}(\boldsymbol{\rho}_i,\boldsymbol{\rho}_j;\hat{\mathbf{r}}_i,-\hat{\mathbf{r}}_{0j}) = \frac{\mathbf{Z}_{ij}(\boldsymbol{\rho}_i,\boldsymbol{\rho}_j;\hat{\mathbf{r}}_i,-\hat{\mathbf{r}}_{0j})}{\Delta S^{pr}_i\mu^{(i)}_\nu\mu^{(j)}_0}, \tag{32}$$

$$\mu_v^{(i)} = \mathbf{n}_i\hat{\mathbf{r}}_i, \quad \mu_0^{(j)} = \mathbf{n}_j\hat{\mathbf{r}}_{0j}, \tag{33}$$

$$\begin{aligned}\mathbf{R}_{ij}(\boldsymbol{\rho}_i,\boldsymbol{\rho}_j;\hat{\mathbf{r}}_i,-\hat{\mathbf{r}}_{0j}) &= \mathbf{R}_i(\boldsymbol{\rho}_i;\hat{\mathbf{r}}_i,-\hat{\mathbf{r}}_{0i})\delta_{ij}\\ &+\mathbf{R}_i(\boldsymbol{\rho}_i;\hat{\mathbf{r}}_i,\hat{\mathbf{r}}_{ji})\mu_{ij}^{(i)}\Delta\Omega_j^{(i)}f_{ext}^2(\boldsymbol{\rho}_i,\boldsymbol{\rho}_j,\mathbf{r}_{ji})\mathbf{R}_j(\boldsymbol{\rho}_j;\hat{\mathbf{r}}_{ji},-\hat{\mathbf{r}}_{0j})(1-\delta_{ij})\\ &+\sum_{\substack{k\neq i\\ k\neq j}}\mathbf{R}_i(\boldsymbol{\rho}_i;\hat{\mathbf{r}}_i,\hat{\mathbf{r}}_{ki})\mu_{ik}^{(i)}\Delta\Omega_k^{(i)}f_{ext}^2(\boldsymbol{\rho}_i,\boldsymbol{\rho}_k,\mathbf{r}_{ki})\mathbf{R}_k(\boldsymbol{\rho}_k;\hat{\mathbf{r}}_{ki},\hat{\mathbf{r}}_{jk})\\ &\times\mu_{kj}^{(k)}\Delta\Omega_j^{(k)}f_{ext}^2(\boldsymbol{\rho}_k,\boldsymbol{\rho}_j,\mathbf{r}_{jk})\mathbf{R}_j(\boldsymbol{\rho}_j;\hat{\mathbf{r}}_{jk},-\hat{\mathbf{r}}_{0j})+\cdots,\end{aligned} \tag{34}$$

$$\mu_{ij}^{(i)} = \mathbf{n}_i\hat{\mathbf{r}}_{ij}, \quad \mu_{ik}^{(i)} = \mathbf{n}_i\hat{\mathbf{r}}_{ik}, \quad \mu_{kj}^{(k)} = \mathbf{n}_k\hat{\mathbf{r}}_{kj}, \tag{35}$$

$$\Delta\Omega_j^{(i)} = \frac{\Delta S_j^{(pr)}(\mathbf{n}_j\hat{\mathbf{r}}_{ji})}{r_{ji}^2}, \quad \Delta\Omega_k^{(i)} = \frac{\Delta S_k^{(pr)}(\mathbf{n}_k\hat{\mathbf{r}}_{ki})}{r_{ki}^2},$$
$$\Delta\Omega_j^{(k)} = \frac{\Delta S_j^{(pr)}(\mathbf{n}_j\hat{\mathbf{r}}_{jk})}{r_{jk}^2}. \tag{36}$$

Here $\Delta S_i^{(pr)}$, $\Delta S_j^{(pr)}$ and $\Delta S_k^{(pr)}$ are the projections of the surface elements ΔS_i, ΔS_j and ΔS_k on the average planes with normals $\mathbf{n}_i$, $\mathbf{n}_j$ and $\mathbf{n}_k$, respectively (see Figs. 2 and 3). $\mathbf{r}_{ij} = \boldsymbol{\rho}_j - \boldsymbol{\rho}_i$, $\mathbf{r}_{ik} = \boldsymbol{\rho}_k - \boldsymbol{\rho}_i$, $\mathbf{r}_{kj} = \boldsymbol{\rho}_j - \boldsymbol{\rho}_k$.

The scattering elements ΔS_i can be considered as a rough surface as well and can be subdivided to smaller surface elements ΔS_{i_1} whose characteristics length ($l_{i_1}^{ch} \sim \sqrt{dS_{i_1}}$) is bigger than the wavelength, much bigger than the extinction length in the medium (i.e., it satisfies the conditions (7), (8), (16)) and much less than the characteristic length l_i^{ch}. Then for the reflection matrix $\mathbf{R}_i$ one can write the equations similar to those for the reflection matrix $\mathbf{R}$ (see Eqs. (31)–(36)):

$$\begin{aligned}\mathbf{R}_i(\boldsymbol{\rho}_i;\hat{\mathbf{r}}_i,-\hat{\mathbf{r}}_{0i}) &= \sum_{i_1 i_2} f_{1ext}^2(\boldsymbol{\rho}_{i_1},\mathbf{r}-\boldsymbol{\rho}_{i_1})\frac{\Delta S_{i_1}^{pr}}{\Delta S_i^{pr}}\\ &\times\frac{\mathbf{R}_{i_1 i_2}^{(1)}(\boldsymbol{\rho}_{i_1},\boldsymbol{\rho}_{i_2};\hat{\mathbf{r}}_i,-\hat{\mathbf{r}}_{0i})}{\mu_v^{(i)}\mu_0^{(i)}}\mu_v^{(i_1)}\mu_0^{(i_2)}f_{1ext}^2(\boldsymbol{\rho}_{i_2},\mathbf{r}_0-\boldsymbol{\rho}_{i_2}),\end{aligned} \tag{37}$$

where $\boldsymbol{\rho}_{i_1} = \boldsymbol{\rho}_i + \Delta\boldsymbol{\rho}_{i_1}$, $\boldsymbol{\rho}_{i_2} = \boldsymbol{\rho}_i + \Delta\boldsymbol{\rho}_{i_2}$, $\Delta\boldsymbol{\rho}_{i_1}$ ($\Delta\boldsymbol{\rho}_{i_2}$) is the radius-vector describing the transition from the coordinate system $\{x_i,y_i,z_i\}$ to the coordinate system $\{x_{i_1},y_{i_1},z_{i_1}\}$ ($\{x_{i_2},y_{i_2},z_{i_2}\}$) (see Fig. 3):

$$\mu_v^{(i_1)} = \mathbf{n}_{i_1}\hat{\mathbf{r}}_i, \quad \mu_0^{(i_2)} = \mathbf{n}_{i_2}\hat{\mathbf{r}}_{0i}, \tag{38}$$

$$\begin{aligned}\mathbf{R}_{i_1 i_2}^{(1)}(\boldsymbol{\rho}_{i_1},\boldsymbol{\rho}_{i_2};\hat{\mathbf{r}}_i,-\hat{\mathbf{r}}_{0i}) &= \mathbf{R}_{i_1}^{(1)}(\boldsymbol{\rho}_{i_1};\hat{\mathbf{r}}_i,-\hat{\mathbf{r}}_{0i})\delta_{i_1 i_2}\\ &+\mathbf{R}_{i_1}^{(1)}(\boldsymbol{\rho}_{i_1};\hat{\mathbf{r}}_i,\hat{\mathbf{r}}_{i_2 i_1})\mu_{i_1 i_2}^{(i_1)}\Delta\Omega_{i_2}^{(i_1)}f_{1ext}^2(\boldsymbol{\rho}_{i_1},\boldsymbol{\rho}_{i_2},\mathbf{r}_{i_2 i_1})\\ &\times\mathbf{R}_{i_2}^{(1)}(\boldsymbol{\rho}_{i_2};\hat{\mathbf{r}}_{i_2 i_1},-\hat{\mathbf{r}}_{0i})(1-\delta_{i_1 i_2})\\ &+\sum_{\substack{i_3\neq i_1\\ i_3\neq i_2}}\mathbf{R}_{i_1}^{(1)}(\boldsymbol{\rho}_{i_1};\hat{\mathbf{r}}_i,\hat{\mathbf{r}}_{i_3 i_1})\mu_{i_1 i_3}^{(i_1)}\Delta\Omega_{i_3}^{(i_1)}f_{1ext}^2(\boldsymbol{\rho}_{i_1},\boldsymbol{\rho}_{i_3},\mathbf{r}_{i_3 i_1})\mathbf{R}_{i_3}^{(1)}\\ &\times(\boldsymbol{\rho}_{i_3};\hat{\mathbf{r}}_{i_3 i_1},\hat{\mathbf{r}}_{i_2 i_3})\\ &\times\mu_{i_3 i_2}^{(i_3)}\Delta\Omega_{i_2}^{(i_3)}f_{1ext}^2(\boldsymbol{\rho}_{i_2},\boldsymbol{\rho}_{i_3},\mathbf{r}_{i_2 i_3})\mathbf{R}_{i_2}^{(1)}(\boldsymbol{\rho}_{i_2};\hat{\mathbf{r}}_{i_2 i_3},-\hat{\mathbf{r}}_{0i})+\cdots,\end{aligned} \tag{39}$$

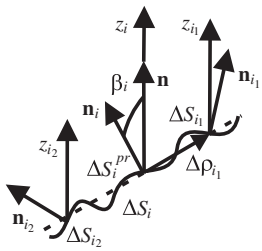

Fig. 3. Schematic representation of surface at second scale.

$$\mu_{i_1 i_2}^{(i_1)} = \mathbf{n}_{i_1}\hat{\mathbf{r}}_{i_1 i_2}, \quad \mu_{i_1 i_3}^{(i_1)} = \mathbf{n}_{i_1}\hat{\mathbf{r}}_{i_1 i_3}, \quad \mu_{i_3 i_2}^{(i_3)} = \mathbf{n}_{i_3}\hat{\mathbf{r}}_{i_3 i_2}, \tag{40}$$

$$\Delta\Omega_{i_2}^{(i_1)} = \frac{\Delta S_{i_2}^{(pr)}(\mathbf{n}_{i_2}\hat{\mathbf{r}}_{i_2 i_1})}{r_{i_2 i_1}^2}, \quad \Delta\Omega_{i_3}^{(i_1)} = \frac{\Delta S_{i_3}^{(pr)}(\mathbf{n}_{i_3}\hat{\mathbf{r}}_{i_3 i_1})}{r_{i_3 i_1}^2},$$
$$\Delta\Omega_{i_2}^{(i_3)} = \frac{\Delta S_{i_2}^{(pr)}(\mathbf{n}_{i_2}\hat{\mathbf{r}}_{i_2 i_3})}{r_{i_2 i_3}^2}. \tag{41}$$

Here $\Delta S_{i_1}^{(pr)}$, $\Delta S_{i_2}^{(pr)}$ and $\Delta S_{i_3}^{(pr)}$ are the projections of the surface elements ΔS_{i_1}, ΔS_{i_2} and ΔS_{i_3} on the average planes with normals $\mathbf{n}_{i_1}$, $\mathbf{n}_{i_2}$ and $\mathbf{n}_{i_3}$, respectively (see Fig. 3). $\mathbf{r}_{i_1 i_2} = \boldsymbol{\rho}_{i_2} - \boldsymbol{\rho}_{i_1}$, $\mathbf{r}_{i_1 i_3} = \boldsymbol{\rho}_{i_3} - \boldsymbol{\rho}_{i_1}$, $\mathbf{r}_{i_3 i_2} = \boldsymbol{\rho}_{i_2} - \boldsymbol{\rho}_{i_3}$.

The subdivision of the surface elements can be further continued providing the relations between the reflection matrices at the different scales where the characteristic lengths satisfy the conditions (7), (8) and (16). At certain scale the reflection matrix can be related to the miscrophysical properties of medium scatterers. In this case the reflection matrix can describe both microphysical and macroscopic properties of medium [3,31,34].

The reflection matrix $\mathbf{R}$ given by Eq. (29) is a conical characteristic introduced for the condition (7) which is not the condition for the far-field approximation (see, for example, [35] and the definition (8)). It is related to the directional reflection matrices $\mathbf{R}_i$ which are defined in the far-field zone (see Eqs. (31) and (34)). The problems regarding the definitions of the characteristic measured by the optical instrument in the near-field zone were discussed in [46]. To avoid similar discussion in this paper, further in the text we assume that the reflection matrix $\mathbf{R}$ can be considered as the directional characteristic as well. Then we have

$$\mathbf{R}_i(\boldsymbol{\rho}_i;\hat{\mathbf{r}}_i,-\hat{\mathbf{r}}_{0i}) = \mathbf{R}_i(\boldsymbol{\rho}_i;\hat{\mathbf{r}},-\hat{\mathbf{r}}_0), \tag{42}$$

$$\begin{aligned}\mathbf{R}(\hat{\mathbf{r}},-\hat{\mathbf{r}}_0) &= \sum_{ij} f_{ext}^2(\boldsymbol{\rho}_i,\mathbf{r}-\boldsymbol{\rho}_i)\frac{\Delta S_i^{pr}}{\Delta S_{obs}^{pr}}\frac{\mathbf{R}_{ij}(\boldsymbol{\rho}_i,\boldsymbol{\rho}_j;\hat{\mathbf{r}},-\hat{\mathbf{r}}_0)}{\mu_v\mu_0}\\ &\times\mu_v^{(i)}\mu_0^{(j)}f_{ext}^2(\boldsymbol{\rho}_j,\mathbf{r}_0-\boldsymbol{\rho}_j),\end{aligned} \tag{43}$$

$$\mu_v^{(i)} = \mathbf{n}_i\hat{\mathbf{r}}, \quad \mu_0^{(j)} = \mathbf{n}_j\hat{\mathbf{r}}_0. \tag{44}$$

Considering $\mathbf{R}$ as the directional characteristic and using the definition of the reflection matrix given by Eq. (29), the element R_{11} of the reflection matrix $\mathbf{R}$ defines surface directional hemispherical reflectance (DHR) $a(\lambda,\vartheta_0)$ (also known as "black sky" or directional albedo):

$$a(\lambda,\vartheta_0,\varphi_0) = \int_0^{2\pi}\int_0^{\pi/2} R_{11}(\lambda,\vartheta_v,\vartheta_0,\phi)\cos\vartheta_v\sin\vartheta_v\, d\vartheta_v\, d\varphi_v.$$

Moreover, the elements R_{11} and R_{21}, R_{31} define the Bidirectional Reflectance Distribution Function (BRDF) and the Bidirectional Polarization Distribution Function (BPDF) [17,18,47]:

$$BRDF = R_{11}, \quad BPDF = \sqrt{R_{21}^2 + R_{31}^2}. \tag{45}$$

Both BRDF and BPDF are used in satellite and airborne remote sensing to characterize surface total and polarized

reflectance angular anisotropy [10–18]. Let us note that till now no averaging has been performed over ensemble of the scattering surface elements. Therefore, the formulas presented in this sections are not related to any specific type of land surfaces. Below in the text we consider the distribution of the scattering elements ΔS_i on the surface, thus dealing mainly with bare soil and desert surfaces.

3. Physical model of BRM (BRDF and BPDF)

The reflection matrix $\mathbf{R}$ in Eq. (31) can be presented as a sum of two other matrices $\mathbf{R}^1$ and $\mathbf{R}^{mult}$:

$$\mathbf{R} = \mathbf{R}^1 + \mathbf{R}^{mult}, \tag{46}$$

$$\mathbf{R}^1(\hat{\mathbf{r}}, -\hat{\mathbf{r}}_0) = \frac{1}{\mu_v \mu_0} \sum_i f^2_{ext}(\boldsymbol{\rho}_i, \mathbf{r}) \frac{\Delta S_i^{pr}}{\Delta S_{obs}^{pr}} \mathbf{R}_i(\boldsymbol{\rho}_i; \hat{\mathbf{r}}, -\hat{\mathbf{r}}_0) \mu_v^{(i)} \mu_0^{(i)} f^2_{ext}(\boldsymbol{\rho}_i, \mathbf{r}_0), \tag{47}$$

$$\mathbf{R}^{mult}(\hat{\mathbf{r}}, -\hat{\mathbf{r}}_0) = \frac{1}{\mu_v \mu_0} \sum_{ij} f^2_{ext}(\boldsymbol{\rho}_i, \mathbf{r}) \frac{\Delta S_i^{pr}}{\Delta S_{obs}^{pr}} \mathbf{R}_{ij}^{mult}(\boldsymbol{\rho}_i, \boldsymbol{\rho}_j; \hat{\mathbf{r}}, -\hat{\mathbf{r}}_0) \mu_v^{(i)} \mu_0^{(j)} f^2_{ext}(\boldsymbol{\rho}_j, \mathbf{r}_0). \tag{48}$$

Here we assume that condition (42) is fulfilled. $\mathbf{R}^1$ corresponds to the radiation scattered by individual surface elements ΔS_i (see Eqs. (37) and (39)) and $\mathbf{R}^{mult}$ describes multiple scattering between different surface elements (double and higher orders of scattering from Eq. (34)). Let us note that $\mathbf{R}^1$ takes into account single and multiple surface scattering and reflection within ΔS_i as well as single and multiple scattering of penetrated into the volumes V_i radiation (Eqs. (37) and (39)).

As it was mentioned before, the rigorous description of both $\mathbf{R}^1$ and $\mathbf{R}^{mult}$ for densely packed media is a very complicated problem (see, for example, [3,31,33]). Further in this paper we develop a physical model for the reflection matrix $\mathbf{R}$ mainly for the purposes of simultaneous retrieval of aerosol and surface properties. We start from Eqs. (31)–(45) and consider a two-scale random rough surface consisting of the small scale roughness superimposed on the large scale roughness. Let us assume that at different scales the surface can be considered as Gaussian surface and that at each scale it can be subdivided into the local surface elements ΔS_i, ΔS_{i_1}, whose characteristic lengths (l_i^{ch} and $l_{i_1}^{ch}$) satisfy the conditions (8) and (16). We consider the two scales in such a way that the characteristics lengths of the small ($l_{ch}^{(1)}$) and large ($l_{ch}^{(0)}$) scales satisfy the conditions:

$$l_{ch}^{(0)} \gg l_{cor}^{(0)}, \quad l_{cor}^{(1)} \ll l_{ch}^{(1)} \ll l_{cor}^{(0)}, \tag{49}$$

where $l_{cor}^{(0)}$ and $l_{cor}^{(1)}$ are the correlation lengths at the large and small scales, respectively. For the Gaussian correlation function the correlation length is related to the mean square surface slope σ^2 and the standard deviation of the surface hight h as follows [1,3]:

$$\sigma^2 = 2\frac{h^2}{l_{cor}^2}. \tag{50}$$

We also assume that the reflection matrices in Eqs. (31)–(45) are already averaged over microphysical properties of medium scatterers (size and space distribution, complex refractive index, shape of medium scatterers, etc.). Then the reflection matrix in Eq. (31) should be averaged over positions, optical properties and orientations of the surface elements at two different scales. This procedure is well-known and is described in the number of papers and books (see, for example, [1–3, 34]). In general, the averaged reflection matrix is obtained as follows:

$$\langle \mathbf{R} \rangle = \int \mathbf{R} f_{pdf}(\boldsymbol{\rho}; \boldsymbol{\rho}^{(1)}; \boldsymbol{\omega}; \boldsymbol{\omega}^{(1)}; \xi; \xi^{(1)})\, d\boldsymbol{\rho}\, d\boldsymbol{\rho}^{(1)} d\boldsymbol{\omega}\, d\boldsymbol{\omega}^{(1)} d\xi\, d\xi^{(1)}. \tag{51}$$

Here $f_{pdf}(\boldsymbol{\rho}; \boldsymbol{\rho}^{(1)}; \boldsymbol{\omega}; \boldsymbol{\omega}^{(1)}; \xi; \xi^{(1)})$ is the probability density function, describing the distribution of the surface elements at two scales over positions ($\boldsymbol{\rho} = (\boldsymbol{\rho}_1, \ldots, \boldsymbol{\rho}_N)$, $\boldsymbol{\rho}^{(1)} = (\boldsymbol{\rho}_1^{(1)}, \ldots, \boldsymbol{\rho}_{N_1}^{(1)})$), orientations ($\boldsymbol{\omega} = (\boldsymbol{\omega}_1, \ldots, \boldsymbol{\omega}_N)$, $\boldsymbol{\omega}^{(1)} = (\boldsymbol{\omega}_1^{(1)}, \ldots, \boldsymbol{\omega}_{N_1}^{(1)})$) and optical properties ($\xi = (\xi_1, \ldots, \xi_N)$, $\xi^{(1)} = (\xi_1^{(1)}, \ldots, \xi_{N_1}^{(1)})$). We assume that: (i) the independent averaging is possible for each scale, (ii) the averaging over optical properties does not depend on the averaging over surface elements orientations and positions, and (iii) the averaging over positions does not depend on the averaging over surface elements orientations. Then, the probability density function $f_{pdf}(\boldsymbol{\rho}; \boldsymbol{\rho}^{(1)}; \boldsymbol{\omega}; \boldsymbol{\omega}^{(1)}; \xi; \xi^{(1)})$ can be presented as the product of the independent probability density functions describing the distribution over positions, orientations and optical properties at two different scales:

$$f_{pdf}(\boldsymbol{\rho}; \boldsymbol{\rho}^{(1)}; \boldsymbol{\omega}; \boldsymbol{\omega}^{(1)}; \xi; \xi^{(1)}) = f_{pdf}^{(0)pos}(\boldsymbol{\rho}) f_{pdf}^{(1)pos}(\boldsymbol{\rho}^{(1)}) \times f_{pdf}^{(0)orien}(\boldsymbol{\omega}) f_{pdf}^{(1)orien}(\boldsymbol{\omega}^{(1)}) f_{pdf}^{(0)opt}(\xi) f_{pdf}^{(1)opt}(\xi^{(1)}). \tag{52}$$

Here f_{pdf}^{pos}, f_{pdf}^{orien} and f_{pdf}^{opt} are the probability density functions describing the distribution over positions, orientations and optical properties, respectively, for two different scales (marked above as 0 and 1).

3.1. Single scattering part of the reflection matrix.

The reflection matrix $\langle \mathbf{R}^1 \rangle$, averaged over orientation, optical properties and position of surface elements, can be presented as follows:

$$\langle \mathbf{R}^1(\hat{\mathbf{r}}, -\hat{\mathbf{r}}_0) \rangle = \frac{1}{\mu_v \mu_0} \times \sum_i \left\langle f^2_{ext}(\boldsymbol{\rho}_i, \mathbf{r}) \frac{\Delta S_{\perp i}^{pr}}{\Delta S_{obs}^{pr}} f^2_{ext}(\boldsymbol{\rho}_i, \mathbf{r}_0) \left\langle \frac{\langle \mathbf{R}_i^1 \rangle_{\xi f_{pdf}^{(1)}}}{\cos \beta_i} \mu_v^{(i)} \mu_0^{(i)} \right\rangle_{\boldsymbol{\omega}_i} \right\rangle_{\boldsymbol{\rho}_i}, \tag{53}$$

$$\Delta S_{\perp i}^{pr} = \Delta S_i^{pr} \cos \beta_i, \quad \cos \beta_i = (\mathbf{n}\mathbf{n}_i). \tag{54}$$

Here $\langle \ldots \rangle_{\boldsymbol{\rho}_i}$ and $\langle \ldots \rangle_{\boldsymbol{\omega}_i}$ give averaging over positions and orientations of the surface elements ΔS_i with probability density functions $f_{pdf}^{(0)pos}(\boldsymbol{\rho}_i)$, $f_{pdf}^{(0)orien}(\boldsymbol{\omega}_i)$:

$$f_{pdf}^{(0)pos}(\boldsymbol{\rho}_i) = \int f_{pdf}^{(0)pos}(\boldsymbol{\rho}_1, .., \boldsymbol{\rho}_i, \ldots, \boldsymbol{\rho}_N) \prod_{k=1, k \neq i}^{N} d\boldsymbol{\rho}_k, \tag{55}$$

$$f_{pdf}^{(0)orien}(\boldsymbol{\omega}_i) = \int f_{pdf}^{(0)orien}(\boldsymbol{\omega}_1, .., \boldsymbol{\omega}_i, \ldots, \boldsymbol{\omega}_N) \prod_{k=1, k \neq i}^{N} d\boldsymbol{\omega}_k. \tag{56}$$

$\langle \mathbf{R}_i^1 \rangle_{\xi f_{pdf}^{(1)}}$ in Eq. (53) is the reflection matrix averaged over orientations, optical properties and positions at the scale 1 as well as over optical properties at the scale 0:

$$\langle \mathbf{R}_i^1 \rangle_{\xi f_{pdf}^{(1)}} = \int \mathbf{R}_i^1 f_{pdf}^{(0)opt}(\xi) f_{pdf}^{(1)pos}(\boldsymbol{\rho}^{(1)}) f_{pdf}^{(1)orien}(\boldsymbol{\omega}^{(1)}) f_{pdf}^{(1)opt}(\xi^{(1)}) \times d\boldsymbol{\rho}^{(1)}\, d\boldsymbol{\omega}^{(1)}\, d\xi\, d\xi^{(1)}. \quad (57)$$

It does not depend on the position of the surface elements ΔS_i. Then, it is possible to perform independent averaging in Eq. (53):

$$\langle \mathbf{R}^1(\hat{\mathbf{r}},-\hat{\mathbf{r}}_0) \rangle = \frac{1}{\mu_v \mu_0} \times \sum_i \left\langle f_{ext}^2(\boldsymbol{\rho}_i,\mathbf{r}) \frac{\Delta S_{\perp i}^{pr}}{\Delta S_{obs}^{pr}} f_{ext}^2(\boldsymbol{\rho}_i,\mathbf{r}_0) \right\rangle_{\boldsymbol{\rho}_i} \left\langle \frac{\langle \mathbf{R}_i^1 \rangle_{\xi f_{pdf}^{(1)}}}{\cos\beta_i} \mu_v^{(i)} \mu_0^{(i)} \right\rangle_{\boldsymbol{\omega}_i}. \quad (58)$$

The term $\sum \langle f_{ext}^2(\boldsymbol{\rho}_i,\mathbf{r}) \Delta S_{\perp i}^{pr} / \Delta S_{obs}^{pr} f_{ext}^2(\boldsymbol{\rho}_i,\mathbf{r}_0) \rangle$ in Eq. (58) gives the fraction of surface which is illuminated and visible simultaneously. It can be considered as the shadowing function f_{shad} which is due to hight distribution of surface elements. For Gaussian random rough surface one can write for f_{shad} [1,4,48,49]:

$$f_{shad}(\sigma,\mu_v,\mu_0) = \frac{1}{1+f_{1shad}(\sigma,\mu_v)+f_{1shad}(\sigma,\mu_0)}, \quad (59)$$

$$f_{1shad}(\sigma,\mu) = \sqrt{\frac{2}{\pi}} \frac{\sigma\sqrt{1-\mu^2}}{2\mu} \exp\left(\frac{\mu^2}{2\sigma^2(1-\mu^2)}\right) - erfc\left(\frac{\mu}{\sigma\sqrt{2(1-\mu^2)}}\right), \quad (60)$$

where σ^2 is the mean square surface slope of Gaussian surface, *erfc* is the complementary error function.

Then, from Eqs. (53)–(60) one can write for the averaged reflection matrix $\langle \mathbf{R}^1(\hat{\mathbf{r}},-\hat{\mathbf{r}}_0) \rangle$:

$$\langle \mathbf{R}^1(\hat{\mathbf{r}},-\hat{\mathbf{r}}_0) \rangle = \frac{1}{\mu_v \mu_0} f_{shad}(\sigma_0,\mu,\mu_0) \times \int_0^{2\pi} d\alpha \int_0^{\pi/2} \langle \mathbf{R}^1(\hat{\mathbf{r}},-\hat{\mathbf{r}}_0) \rangle_{\xi f_{pdf}^{(1)}} \mu_v' \mu_0' f_{shad}^{orien}(\mu_v',\mu_0') \times f_{pdf}^{(0)orien}(\sigma_0,\alpha,\beta) \tan\beta\, d\beta, \quad (61)$$

$$f_{shad}^{orien}(\mu_v',\mu_0') = \begin{cases} 0, & \mu_v' \le 0,\ \mu_0' \le 0, \\ 1, & \mu_v' > 0,\ \mu_0' > 0, \end{cases} \quad (62)$$

$$\mu_v' = \cos\beta\mu_v + \sin\beta\sqrt{1-\mu_v^2}\cos(\alpha-\phi_v), \quad (63)$$

$$\mu_0' = \cos\beta\mu_0 + \sin\beta\sqrt{1-\mu_0^2}\cos(\alpha-\phi_0), \quad (64)$$

where φ_0 and φ_v are the solar and viewing azimuth angles, the function $f_{shad}^{orien}(\mu_v',\mu_0')$ describes shadowing which is due to the orientation of the surface element.

For Gaussian random rough surface the probability density function of surfaces slopes $f_{pdf}^{(0)orien}(\sigma_0,\alpha,\beta)$ is described as follows [1,3]:

$$f_{pdf}^{(0)orien}(\sigma_0,\alpha,\beta) = \frac{1}{2\pi\sigma_0^2\cos^3\beta} \exp\left(-\frac{\tan^2\beta}{2\sigma_0^2}\right), \quad (65)$$

$$\int_0^{2\pi} d\alpha \int_0^{\pi/2} f(\sigma,\alpha,\beta) \sin\beta\, d\beta = 1. \quad (66)$$

In general, the matrix $\langle \mathbf{R}^1 \rangle_{\xi f_{pdf}^{(1)}}$ in Eq. (61) can be further decomposed into two other matrices:

$$\langle \mathbf{R}^1 \rangle_{\xi f_{pdf}^{(1)}} = \delta_{Fr} \langle \mathbf{R}^{1Fr} \rangle_{\xi f_{pdf}^{(1)}} + \langle \mathbf{R}^{1diff} \rangle_{\xi f_{pdf}^{(1)}}, \quad (67)$$

where $\mathbf{R}^{1Fr}$ describes single surface Fresnel reflection, $\mathbf{R}^{1diff}$, referred hereafter as the diffuse part of the reflection matrix, takes into account the rest part of scattering and reflection. In Eq. (67) we take into account the fact that only the fraction of surface δ_{Fr} can provide Fresnel reflection:

$$\delta_{Fr} = \frac{\Delta S_i^{Fr}}{\Delta S_i}, \quad (68)$$

where ΔS_i^{Fr} is the surface area with Fresnel reflection, ΔS_i is the surface area of the i-th surface element.

Since we assume that at the second scale the surface also can be considered as Gaussian surface, Fresnel part $\langle \mathbf{R}^{1Fr} \rangle_{\xi f_{pdf}}$ of the reflection matrix can be obtained in the same way as for Gaussian rough surface within Kirchoff approximation in geometric optic limit [1,3]:

$$\langle \mathbf{R}^{1Fr}(\beta,\hat{\mathbf{r}},-\hat{\mathbf{r}}_0) \rangle_{\xi f_{pdf}^{(1)}} = \frac{1}{4\mu_v'\mu_0'} \frac{1}{2\sigma_1^2\cos^4\beta'} \exp\left(-\frac{\tan^2\beta'}{2\sigma_1^2}\right) \times \langle \mathbf{Z}^{Fr}(m,\hat{\mathbf{r}},-\hat{\mathbf{r}}_0) \rangle_{\xi,\xi_1} f_{shad}(\sigma_1,\mu_v',\mu_0'). \quad (69)$$

Here $\mathbf{Z}^{Fr}$ is Fresnel phase matrix (see Appendix B, Eqs. (95)–(103)), m is the complex refractive index of medium providing Fresnel reflection; σ_1^2 is the mean surface slope at the second scale, $f_{shad}(\sigma_1,\mu_v',\mu_0')$ is the shadowing function at the second scale defined by Eq. (59); $\cos\beta' = \frac{\mu_0'+\mu_v'}{2\sin(\gamma'/2)}$, γ is the scattering angle ($\cos\gamma = -\hat{\mathbf{r}}\hat{\mathbf{r}}_0$).

To describe the diffuse part of the matrix $\langle \mathbf{R}^{1diff} \rangle_{\xi f_{pdf}^{(1)}}$ we use the fact that a complex system of scatterers gives a bell-shaped angular profile of the degree of linear polarization, essential depolarization ($R_{11}^{1diff} > R_{22}^{1diff}$) and, very often, a flat intensity angular profile in a wide range of scattering angles [33,50–52]. According to these facts in this paper we consider $\langle \mathbf{R}^{1diff} \rangle_{\xi f_{pdf}^{(1)}}$ in the following simplified form:

$$\langle \mathbf{R}^{1diff} \rangle_{\xi f_{pdf}^{(1)}} = \mathbf{L}(\eta_v) \begin{pmatrix} a_{iso}(\lambda) & -\Delta_p(\lambda)\sin^2\gamma & 0 & 0 \\ -\Delta_p(\lambda)\sin^2\gamma & 0 & 0 & 0 \\ 0 & 0 & 0 & 0 \\ 0 & 0 & 0 & 0 \end{pmatrix} \mathbf{L}(\eta_{inc}), \quad (70)$$

where γ is the scattering angle, λ is the wavelength of the incident and scattered radiation, a_{iso} is the wavelength dependent averaged albedo of the surface elements, and the parameter Δ_p is the wavelength dependent model parameter which allows modifying the value of polarization. The possibility of using more physical model for $\langle \mathbf{R}^{1diff} \rangle_{\xi f_{pdf}^{(1)}}$ will be discussed later in the paper.

3.2. Multiple scattering part of the reflection matrix

The rigorous description of the matrix $\mathbf{R}^{mult}$ in Eqs. (34), (46) is the most difficult part of the considered problem. Here we use the order of scattering technique and simplify the terms corresponding to the second and the third orders of scattering.

According to Eqs. (48)–(52) one can write for the averaged reflection matrix $\mathbf{R}^{mult}$:

$$\langle \mathbf{R}^{mult}(\hat{\mathbf{r}},-\hat{\mathbf{r}}_0)\rangle = \frac{1}{\mu_v\mu_0} \times\left\langle \sum_{ij} f^2_{ext}(\boldsymbol{\rho}_i,\mathbf{r})\frac{\Delta S^{pr}_{\perp i}}{\Delta S^{pr}_{obs}}\left\langle \frac{\langle \mathbf{R}^{mult}_{ij}(\boldsymbol{\rho}_i,\boldsymbol{\rho}_j;\hat{\mathbf{r}},-\hat{\mathbf{r}}_0)\rangle_{\xi f^{(1)}_{pdf}}}{\cos\beta_i}\mu^{(i)}_v\mu^{(j)}_0\right\rangle_{\boldsymbol{\omega}} f^2_{ext}(\boldsymbol{\rho}_j,\mathbf{r}_0)\right\rangle_{\boldsymbol{\rho}}. \tag{71}$$

Here the averaged term $\langle\langle \mathbf{R}^{mult}_{ij}(\boldsymbol{\rho}_i,\boldsymbol{\rho}_j;\hat{\mathbf{r}},-\hat{\mathbf{r}}_0)\rangle_{\xi f^{(1)}_{pdf}}\mu^{(i)}_v\mu^{(j)}_0/\cos\beta_i\rangle_{\boldsymbol{\omega}}$ depends, in general, on the positions of the surface elements. In other words, to average rigorously the term, one must take into account the correlation on surface elements positions that considerably complicates the problem. Therefore, let us make three other assumptions: (iv) let us assume that the position of a surface element ΔS_i does not depend on the position of a surface element ΔS_j; (v) the reflection matrix $\langle \mathbf{R}^{mult}_{ij}\rangle$ depends mainly on the relative distance between the surface elements $\mathbf{r}_{ij}=\boldsymbol{\rho}_j-\boldsymbol{\rho}_i$:

$$\langle \mathbf{R}^{mult}_{ij}(\boldsymbol{\rho}_i,\boldsymbol{\rho}_j;\hat{\mathbf{r}},-\hat{\mathbf{r}}_0)\rangle \approx \langle \mathbf{R}^{mult}_{ij}(\mathbf{r}_{ij};\hat{\mathbf{r}},-\hat{\mathbf{r}}_0)\rangle, \tag{72}$$

and (vi) for the extinction function $f^2_{ext}(\boldsymbol{\rho}_j,\mathbf{r}_0)$ it is possible to separate the dependence on $\boldsymbol{\rho}_i$ and $\mathbf{r}_{ij}$:

$$f^2_{ext}(\boldsymbol{\rho}_j,\mathbf{r}_0)\approx f^2_{ext}(\boldsymbol{\rho}_i,\mathbf{r}_0)f^2_{ext}(\mathbf{r}_{ij},\mathbf{r}_0). \tag{73}$$

With these three additional assumptions, Eq. (71) can be simplified as follows:

$$\langle \mathbf{R}^{mult}(\hat{\mathbf{r}},-\hat{\mathbf{r}}_0)\rangle = \frac{1}{\mu_v\mu_0}\sum_i\left\langle f^2_{ext}(\boldsymbol{\rho}_i,\mathbf{r})\frac{\Delta S^{pr}_{\perp i}}{\Delta S^{pr}_{obs}}f^2_{ext}(\boldsymbol{\rho}_i,\mathbf{r}_0)\right\rangle_{\boldsymbol{\rho}_i} \times\sum_j\left\langle \frac{\langle \mathbf{R}^{mult}_{ij}(\mathbf{r}_{ij};\hat{\mathbf{r}},-\hat{\mathbf{r}}_0)\rangle_{\xi f^{(1)}_{pdf}}}{\cos\beta_i}\mu^{(i)}_v\mu^{(j)}_0 f^2_{ext}(\boldsymbol{\rho}_{ij},\mathbf{r}_0)\right\rangle_{\Delta\mathbf{r},\boldsymbol{\omega}}. \tag{74}$$

Here the term $\langle\cdots\rangle_{\boldsymbol{\rho}_i}$ is the shadowing function which can be given by Eq. (59). To simplify further Eq. (74) we take into account the fact that due to the averaging the term $\langle\ldots.\rangle_{\Delta\mathbf{r},\boldsymbol{\omega}}$ should have slight dependence on φ_v, ϑ_v, φ_0, ϑ_0. In the paper we consider it as geometry independent parameter. Also, here we consider only the element R^{mult}_{11} of the reflection matrix $\mathbf{R}^{mult}$ assuming that all other elements are much less than the corresponding elements of the reflection matrix $\mathbf{R}^1$. Then, for the reflection matrix $\langle \mathbf{R}^{mult}\rangle$ we can write

$$\langle \mathbf{R}^{mult}(\hat{\mathbf{r}},-\hat{\mathbf{r}}_0)\rangle = \frac{1}{\mu_v\mu_0}f_{shad}(\sigma_0,\mu,\mu_0)\mathbf{R}^{iso}, \tag{75}$$

$$\mathbf{R}^{iso}=\begin{pmatrix} b_{iso}(\lambda) & 0 & 0 & 0\\ 0 & 0 & 0 & 0\\ 0 & 0 & 0 & 0\\ 0 & 0 & 0 & 0\end{pmatrix}. \tag{76}$$

The wavelength dependent parameter b_{iso} can be related to the parameter a_{iso} from Eq. (70). Indeed, since $R^{1diff}_{11}\gg R^{1Fr}_{11}$ in a wide angular range (R^{1Fr}_{11} may be much bigger than R^{1diff}_{11} in a very narrow angular range close to specular reflection direction for the media which provide strong Fresnel reflection), then according to the order of scattering expansion (see, for example, Eq. (34)), one can write for b_{iso}:

$$b_{iso}(\lambda)=k_1a^2_{iso}(\lambda)+k_2a^3_{iso}(\lambda)+\cdots, \tag{77}$$

where $k_1,k_2,\ldots$ are the wavelength independent coefficients, which, in general, are result of averaging of order of scattering terms over the surface elements positions and orientations (see Eqs. (34), (70), (74)).

3.3. Reflection model: some remarks

According to the results, presented in the previous sections, the reflection matrix $\langle\mathbf{R}\rangle$ averaged over ensemble of the surface elements can be presented as a sum of three matrices:

$$\langle\mathbf{R}\rangle=\delta_{Fr}\langle\mathbf{R}^{1Fr}\rangle+\langle\mathbf{R}^{1diff}\rangle+\langle\mathbf{R}^{mult}\rangle, \tag{78}$$

where the parameter δ_{Fr} corresponds to the fraction of surface which can provide Fresnel reflection (see Eq. (68)).

The matrix $\langle\mathbf{R}^{1Fr}\rangle$ describes Fresnel part of the scattered radiation. Eqs. (61)–(65) and Eqs. (69). This reflection matrix depends on such parameters as the complex refractive index $m(\lambda)$ of the medium providing Fresnel reflection, and the mean square surface slopes σ^2_0 and σ^2_1 at two different scales (see Eq. (49) for the characteristic length determination for each scale).

The matrix $\langle\mathbf{R}^{1diff}\rangle$ is described by Eqs. (61)–(65) and Eq. (70). There are three model parameters for this part of the reflection matrix: the wavelength dependent averaged albedo of the surface element $a_{iso}(\lambda)$; the wavelength dependent free model parameter $\Delta_p(\lambda)$ which allows reducing the amplitude of the bell-shaped polarization pattern; the mean square surface slope σ^2_0 at the first scale.

The matrix $\langle\mathbf{R}^{mult}\rangle$ describes multiple scattering between different surface elements. The estimation of the contribution of this part of the reflection matrix is given by Eq. (76). According to Eq. (76) $\langle\mathbf{R}^{mult}\rangle$ depends on the wavelength dependent parameter $b_{iso}(\lambda)$ (Eq. (77)), and the mean square surface slope σ^2_0 at the first scale of the medium.

Thus, in general, there are seven parameters of the model: $a_{iso}(\lambda)$, σ_0, $b_{iso}(\lambda)$, δ_{Fr}, $\Delta_p(\lambda)$, σ_1, and $m(\lambda)$. Four out of seven parameters are wavelength dependent parameters. The number of wavelength dependent parameters can be considerably reduced. In particularly, for Earth land surfaces the wavelength dependence of $\langle\mathbf{R}^{1Fr}\rangle$ is not considerable in visible and infrared spectral regions comparing with the wavelength dependence of other two matrices $\langle\mathbf{R}^{1diff}\rangle$ and $\langle\mathbf{R}^{mult}\rangle$. Moreover, for land surface

it is possible to fix the value of m. Usually, it is taken equal to 1.5 [17]. Also, the surface polarized reflectance is almost independent on the wavelength as it follows from the remote sensing of land surfaces [16–18]. Therefore, very often it is possible to neglect the spectral dependence of the parameter $\Delta_p(\lambda)$. And finally, according to Eq. (77), the spectral dependence of b_{iso} can be described by the spectral dependence of a_{iso}. Thus, for the cases where the double-scattering approximation is valid, instead of the wavelength dependent parameter $b_{iso}(\lambda)$ one can use wavelength independent parameter k_1: $b_{iso}(\lambda) = k_1 a_{iso}^2(\lambda)$. Taking into account the above mentioned reasons, very often it is possible to use six parameters: $a_{iso}(\lambda)$, σ_0, k_1, δ_{Fr}, Δ_p, σ_1 ($m(\lambda) = 1.5$), one of which ($a_{iso}(\lambda)$) is wavelength dependent parameter.

Let us also note that it is possible to reduce further the number of the parameters. In particular, if we do not take into account the surface roughness at the second scale we can use only five parameters in the model ($a_{iso}(\lambda)$, σ_0, k_1 (or $b_{iso}(\lambda)$ in general), δ_{Fr}, Δ_p). Also, when Fresnel reflection contribution is small, the number of the parameters is reduced to four ($a_{iso}(\lambda)$, σ_0, k_1, Δ_p). If in addition it is not necessary to take into account the polarization of scattered radiation, one can work with three model parameters ($a_{iso}(\lambda)$, σ_0,k_1 (if necessary $b_{iso}(\lambda)$)).

In the next section we deal with the six parameter model ($a_{iso}(\lambda)$, σ_0, k_1, δ_{Fr}, Δ_p, σ_1 ($m(\lambda) = 1.5$)), which takes into account scattering between different surface elements. The model is tested on airborne RSP (Research Scanning Polarimeter) and satellite POLDER (Polarization and Directionality of the Earth's Reflectances) BRDF and BPDF measurements.

4. Fitting to RSP and POLDER BRDF/BPDF measurements

In Refs. [19,20] three aspects for BRDF and BPDF models were formulated, which are important for accurate description of the surface signal as well as for accurate separation of atmospheric signal from the surface signal: (i) there must be known constraints on and invariances of the spectral and angular dependences of the BRDF and BPDF; (ii) BRDF and BPDF models should be able to correctly describe the surface signal with the geometry of the measurements (flexibility), as well as (iii) for all other geometries (predictability). In this section we use multi-angle, multi-spectral photopolarimetric airborne RSP measurements and satellite POLDER measurements to investigate the performance of the above presented model in terms of the three aspects for BRDF and BPDF models.

RSP measures intensity and polarization characteristics in a wide range of viewing zenith angles ($\pm 60^\circ$ from the zenith direction) in nine spectral bands in the range 410–2260 nm [25–27]. We used RSP data obtained during the ALIVE (Aerosol Lidar Validation Experiment) measurement campaign performed in Oklahoma (USA, Southern Great Plains) in September of 2005 [15]. There are several flights in the ALIVE campaign with measurements at low altitude over land (about 200–600 m). These measurements provide good opportunity for testing and further validating models of the BRDF and BPDF for Earth surfaces.

POLDER measures intensity and polarization characteristics of radiation scattered by coupled surface-atmosphere system at 16 different viewing zenith angle and at different wavelengths from visible till near infrared regions (there are nine spectral bands for intensity: 443, 490, 565, 670, 763, 765, 865, 910, 1020 nm; and three bands for linear polarization measurements: 490, 670, 865 nm) [21,22]. At present time a big database of POLDER measurements for BRDF and BPDF characterization for different kinds of Earth surfaces is available [53].

Figs. 4 and 5 show the results of fitting the model, presented in the paper, to RSP measurements. Here the solid lines correspond to RSP measurements for bare soil for two different flights and three different wavelengths (see Table 2 and the caption for Fig. 4). The flights were carried out over the same area at different times during the same day (see [15,54] for details). Dashed lines correspond to the values of BRDF and BPDF calculated at the best fitted parameters (see Table 2) using Eqs. (61)–(78).

The physical model clearly shows the spectral dependence of the model parameters (the first aspect for BRDF and BPDF models). The fitting in Figs. 4 and 5 was performed for the case when two model parameters a_{iso} and Δ_p are wavelength dependent. One can see from

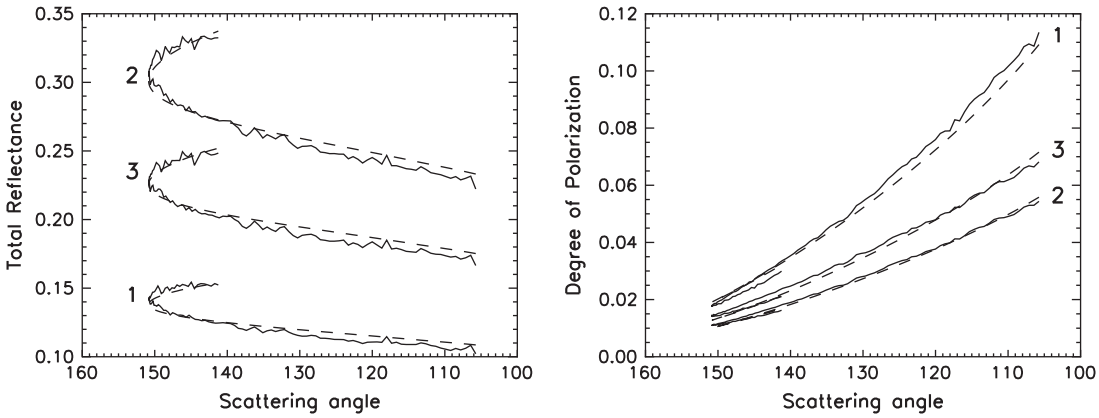

Fig. 4. Angular dependences of the total reflectance and the degree of linear polarization for bare soil surface and for the Flight 1 (see Table 2). The solid curves 1, 2 and 3 correspond to RSP data obtained in the channel 4 ($\lambda = 670$ nm), channel 7 ($\lambda = 1589$ nm) and channel 9 ($\lambda = 2264$ nm), respectively. The dashed curves show the angular dependences of the model BRDF and the degree of linear polarization ($BPDF/BRDF$) for corresponding wavelength.

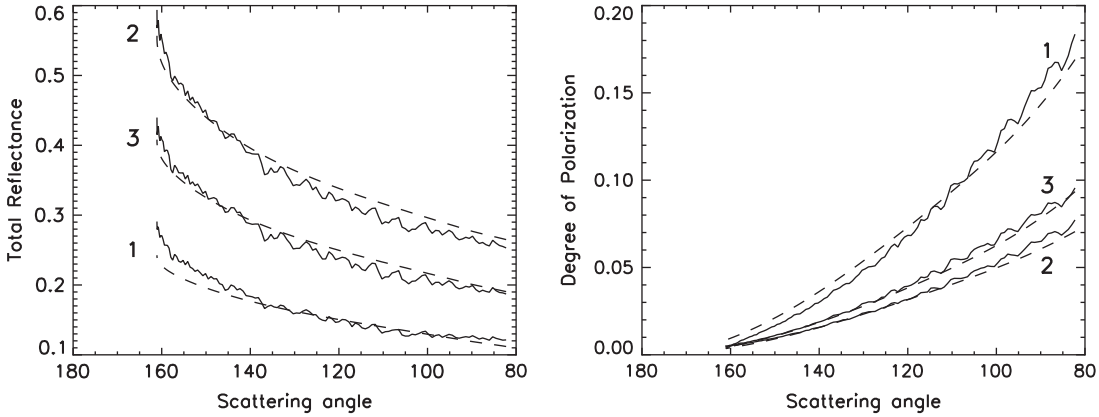

Fig. 5. The same angular profiles as in Fig. 4 but for the Flight 2 (see Table 2).

Table 2
Fitting to RSP measurements.

Model parameters ($m=1.5$)	Flight 1	Flight 2
	$\vartheta_0=42.68^\circ$, $\phi=45.95^\circ(225.95^\circ)$	$\vartheta_0=60.8^\circ$, $\phi=21.8^\circ(201.8^\circ)$
a_{iso}(670 nm)	0.144	0.167
a_{iso}(1589 nm)	0.317	0.343
a_{iso}(2264 nm)	0.238	0.265
σ_1^2	0.378	0.517
k_1	0.069	0.369
δ_{Fr}	0.348	0.380
Δ_p(670 nm)	0.009	0.013
Δ_p(1589 nm)	0.011	0.013
Δ_p(2264 nm)	0.010	0.011
σ_2^2	0.111	0.121

Table 2 that the polarization parameter Δ_p depends slightly on the wavelength confirming the fact that the surface polarized reflectance almost spectrally neutral. Nevertheless, for highly accurate measurements similar to those provided by RSP instrument, it may be useful to take it into account.

Let us note that accuracy of the fit (less than 2% for total reflectance and less than 0.2% for the degree of linear polarization) is within RSP intensity and polarisation measurement error [25–27]. Therefore, we can conclude that the second aspect is fulfilled for the presented model.

Comparing the best fitted parameters obtained for the two different flights (see Table 2), one can notice that the model parameters a_{iso}, δ_{Fr}, Δ_p, σ_1 are almost the same (the third aspect is fulfilled), whereas the parameters σ_0, k_1 differ quite considerably. This is due to the fact that the soil surfaces considered here are azimuthally anisotropic plowed surfaces with different roughness at different azimuthal directions. The model parameter σ_0 describes the surface roughness and the parameter k_1 depends on the surface roughness.

Figs. 6 and 7 show the results of fitting the model presented in the paper to POLDER BRDF and BPDF measurements. POLDER polarization measurements accuracy is less than that for RSP instrument. Therefore POLDER is almost insensitive to the spectral dependence of the land surface polarized reflectance and POLDER BPDF database contains the surface polarized reflectance for 865 nm. As a result, we have only one spectrally dependent parameter $a_{iso}(\lambda)$ (averaged albedo of a surface element) (see Table 3). Here the accuracy of the fit is also within the accuracy of measurements that brings us to the conclusion that the first and the second aspects are fulfilled for the physical model.

Comparing the best fitted parameters retrieved for the geometries for Figs. 6 and 7, one can see the result similar to that for RSP measurements: the parameter σ_0 is different for different geometries whereas the model parameters a_{iso}, δ_{FR}, Δ_p, σ_1, k_1 are almost the same (the third aspect is fulfilled). Indeed, the geometries of the measurements in Figs. 6 and 7 differ considerably by the relative azimuth (see Table 3). It is highly probable that differences in parameters σ_0 are caused by the azimuth anisotropy of the scattering surface.

One can notice essential difference between the retrieved parameters from RSP and POLDER measurements (see Tables 2 and 3). The reason of this is that POLDER and RSP data we used in our studies are related to different type of surfaces: Sahara desert and Oklahoma bare soil surfaces, respectively. Another reason is that the spatial resolution of RSP instrument for the used data was about 3 m (at the airplane altitude 200 m over land) and the spatial resolution of POLDER was 6 km. As a result, the retrieved parameters σ_1, σ_2 presented in Tables 2 and 3 describe the effective surface roughness within different scales for RSP and POLDER.

Fig. 8 shows the results of POLDER measurements for the geometry close to the backscattering direction. One can see here more considerable growth of the total reflectance with approaching to the exact backscattering direction. Such angular dependence is well known as “opposition” or “hot spot” effect. There are two physical reasons for this effect: the first one is because of the shadowing effect (see, for example, [30,55]), another one is because of the coherent backscattering effect (see, for example, [29,34,41–45]). The spectral dependence of the opposition effect is different for different mechanisms. If the opposition effect has geometrical-optic nature (because of the shadowing) than it becomes less pronounced for the bright surfaces since the multiple scattering reduce the effect of the shadowing. In the

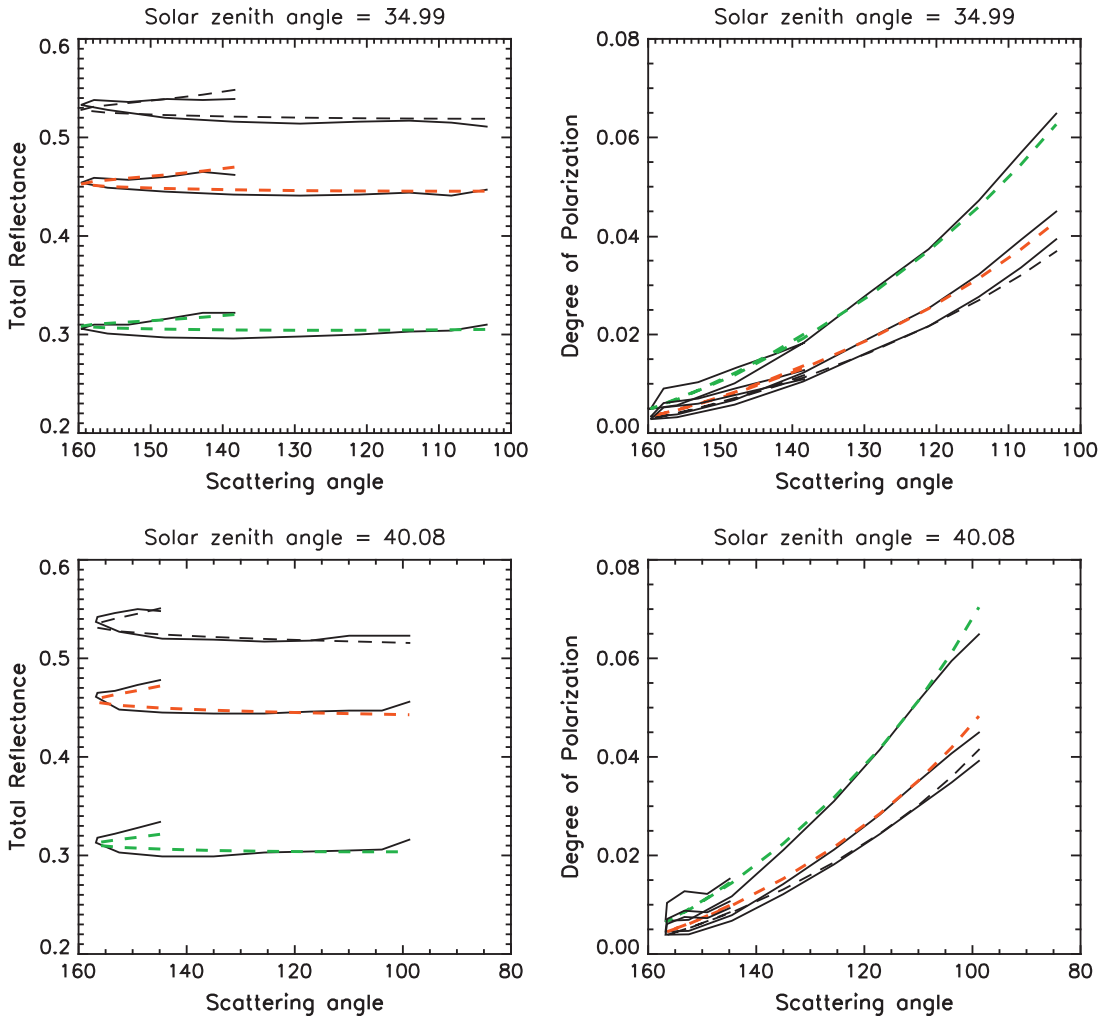

Fig. 6. Angular dependences of the total reflectance and the degree of linear polarization for desert surface and for POLDER geometry 1 (see Table 3). The solid curves correspond to POLDER data. The dashed curves show the angular dependences of the model BRDF and the degree of linear polarization (*BPDF*/*BRDF*) for $\lambda = 565$nm (green curve), $\lambda = 670$nm (red curve) and $\lambda = 865$ nm (black curve). (For interpretation of the references to color in this figure caption, the reader is referred to the web version of this article.)

case when the opposition effect is produced by the coherent backscattering phenomena, it manifests itself more considerably for the bright surfaces. Since the desert surface considered here is a very bright surface, the coherent backscattering mechanism seems to be the most probable candidate for explanation of growth of the total reflectance in the backscattering region. Accurate physical description of the coherent backscattering effect (see, for example, [45]) may complicate the BRDF and BPDF models. The way to take this effect into account in our model is under consideration now. Let us note that existent semi-empirical models deal with this problem in the simplified manner: to describe the hot spot effect the simple semi-empirical functions are used [12,28]. The importance of proper description of the "opposition" ("hot spot") effect for the problem of aerosol retrieval over land have to be considered yet.

Resuming, from Figs. 4–8 we can conclude that, in general, the model satisfies the requirements applied on BRDF and BPDF models for aerosol retrieval over land [19,20]. The backscattering region may be an exception. Here the coherent backscattering effect can manifest itself, whose physical description requires modifications of the matrix $\langle \mathbf{R}^{1diff} \rangle$ of the model. More detail model testing on larger set of measurements will be the subject of further investigation.

5. Conclusions and discussion

Physical model for the reflection matrix for random rough surfaces has been presented in the previous sections. The model is derived from the general solution of the electromagnetic scattering problem by random media. Deriving our model we substitute the real medium with the effective medium corresponding to the used assumptions and approximations. The more realistic assumptions we make, the more the parameters of the effective medium are related to the physical parameters of a real medium. Since we derived our model directly from the

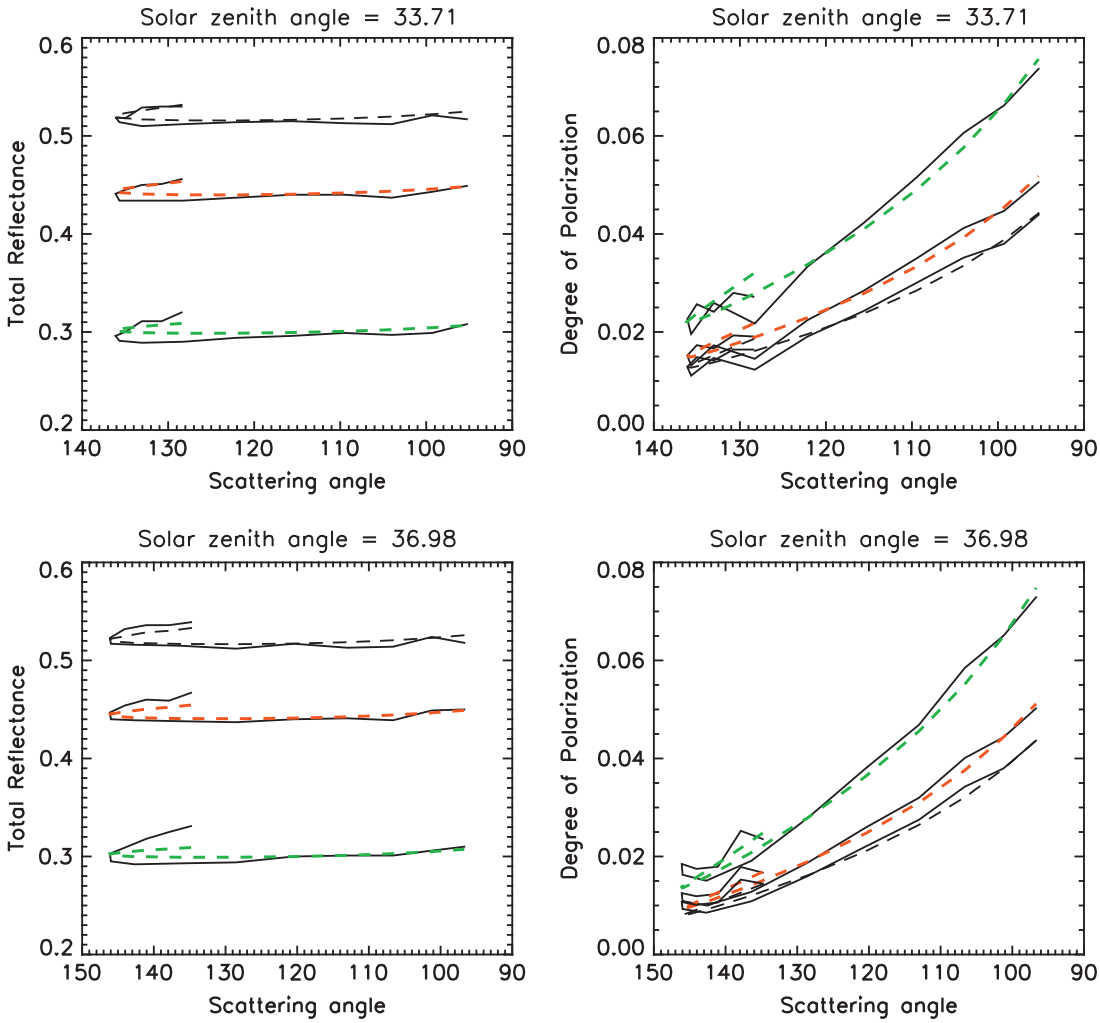

Fig. 7. The same angular profiles as in Fig. 6 but for POLDER geometry 2 (see Table 3).

Table 3
Fitting to POLDER measurements.

Model parameters (m=1.5)	POLDER (geometry 1, Fig. 6) $\vartheta_0=35^\circ$, $\vartheta_0=40.1^\circ$ $\phi=0-45^\circ$ ($\phi=238-306^\circ$)	POLDER (geometry 2, Fig. 7) $\vartheta_0=33.7^\circ$, $\vartheta_0=37^\circ$ $\phi=56-229^\circ$	POLDER (geometry 3, Fig. 8) $\vartheta_0=36.46^\circ$ $\phi=8-35^\circ$ ($\phi=265-354^\circ$)
$a_{iso}(565)$	0.309	0.319	0.313
$a_{iso}(670)$	0.457	0.474	0.458
$a_{iso}(865)$	0.533	0.556	0.533
σ_1^2	0.06	0.012	0.06
k_1	0.014	0.015	0.014
δ_{Fr}	0.502	0.544	0.502
Δ_p(870 nm)	0.009	0.010	0.009
σ_2^2	0.341	0.347	0.341

general solution of the electromagnetic scattering problem by random media, further improvement of the model is possible at each step. For example, the matrix for description of the diffuse part of radiation $\langle \mathbf{R}^{1diff} \rangle$ (Eq. (70)) can be characterized more accurately using radiative transfer equations for dense media (see, for example, [3,31]). More accurate description is possible also for the matrix $\mathbf{R}^{iso}$ (Eq. (76)) describing multiple

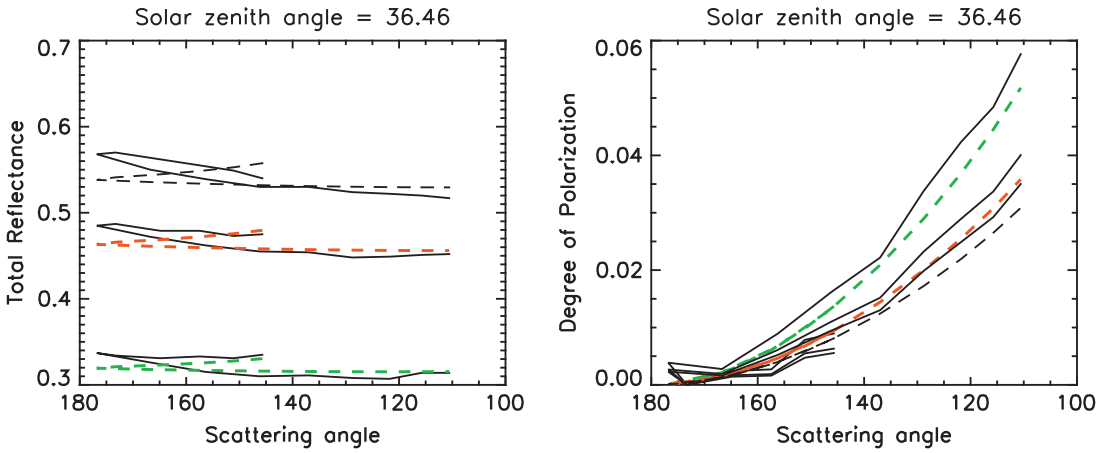

Fig. 8. The same angular profiles as in Fig. 6 but for POLDER geometry 3 (see Table 3).

scattering between different scattering elements. Such improvements provide more physical relation between the model parameters and the medium properties. It would have an advantage if the retrieval of the physical properties of surfaces was the main goal. Such detailed physical description of the surface reflection can be more complicated than the radiative transfer in the atmosphere. Therefore, for the purpose of aerosol properties retrieval over land, it is very important to find optimal balance between the physical nature of BRM models and the possibility to use these models into inversion algorithms for coupled surface-atmosphere system.

To demonstrate the performance of the model, we presented the results of fitting for limited numbers of geometries and types of surfaces. From the comparison with RSP and POLDER measurements we can conclude that the presented model is able to follow the spectral and angular behaviour of the signal scattered by the real medium, and satisfies the requirements applied on BRDF and BPDF models for aerosol retrieval over land. More comprehensive analysis for much bigger numbers of geometries and surface types should still be done to test the model. In the backscattering region the presented model does not give as good fit to POLDER measurements as for other geometries. The most probable reason of this is that we do not describe the coherent backscattering effect in the matrix $\langle \mathbf{R}^{1diff} \rangle$. To overcome this difficulty we either can use the semi-empirical functions (see, for example, [28]) or obtain a simplified formula for coherent backscattering peak profile from the theory of coherent backscattering [41–45].

One of the advantages of the presented model is based on the fact that there is a possibility to control the spectral dependence and the range of variability of the model parameters. This should improve the accuracy of aerosol properties retrieval over land. Another advantage is due to the fact that the model describes simultaneously the surface total and polarized reflectance (the BRDF model parameters are related to the BPDF model parameters). That provides more accurate separation of atmospheric and surface signals. Moreover, the model allows surface properties characterization since it is sensitive to the surface albedo, surface roughness and the fraction of Fresnel reflection. Finally, on the basis of the comparison with RSP, POLDER measurements further improvement of the model is possible. Overall, we can conclude that presented results demonstrate a big potential of the physically based BRM models for simultaneous aerosol and surface characterization on the basis of satellite and airborne measurements.

Acknowledgements

We are grateful to M. Mishchenko, V. Tishkovets, M. Herman, D. Tanré and F.-M. Bréon for useful discussions. Also, we thank D. Tanré and F.-M. Bréon for providing us with POLDER BRDF/BPDF database. This research was supported by the Dutch User Support Program (USP) under project GO-AO/03.

Appendix A. Green's function asymptotic

The free space dyadic Green's function $\overleftrightarrow{G}_0$ for the electromagnetic wave propagation and scattering problem can be defined as follows (see, for example, [3,34]):

$$\overleftrightarrow{G}_0(\mathbf{r}',\mathbf{r}'') = \left(\overleftrightarrow{I} + \frac{\nabla_{\mathbf{r}'} \otimes \nabla_{\mathbf{r}'}}{k^2}\right) g(\mathbf{r}',\mathbf{r}''), \tag{79}$$

where

$$g(\mathbf{r}',\mathbf{r}'') = \frac{\exp\,(ik|\mathbf{r}'-\mathbf{r}''|)}{4\pi|\mathbf{r}'-\mathbf{r}''|}. \tag{80}$$

If $|\mathbf{r}'| \gg |\mathbf{r}''|$ and $k|\mathbf{r}'| \gg 1$, then one can write:

$$\overleftrightarrow{G}_0(\mathbf{r}',\mathbf{r}'') = (\overleftrightarrow{I} - \hat{\mathbf{r}}' \otimes \hat{\mathbf{r}}')g(\mathbf{r}',\mathbf{r}''). \tag{81}$$

Let us note that in the coordinate system $\{x_1,y_1,z_1\}$ with z_1-axis directed along the vector $\mathbf{r}'$ the components

of the tensor $(\overleftrightarrow{I}-\hat{\mathbf{r}}'\otimes\hat{\mathbf{r}}')$ are defined as follows:

$$(\overleftrightarrow{I}-\hat{\mathbf{r}}'\otimes\hat{\mathbf{r}}')=\mathbf{M}_z(\hat{\mathbf{z}},\hat{\mathbf{r}}')\begin{pmatrix}1&0&0\\0&1&0\\0&0&0\end{pmatrix}\mathbf{M}_z^{-1}(\hat{\mathbf{z}},\hat{\mathbf{r}}'),\tag{82}$$

where $\mathbf{M}_z(\hat{\mathbf{z}},\hat{\mathbf{r}}')$ is the rotation matrix from the coordinate system $\{x_1,y_1,z_1\}$ to the reference coordinate system $\{x,y,z\}$:

$$\mathbf{M}_z(\hat{\mathbf{z}},\hat{\mathbf{r}}')=\begin{pmatrix}\hat{\mathbf{x}}\hat{\mathbf{x}}_1&\hat{\mathbf{x}}\hat{\mathbf{y}}_1&\hat{\mathbf{x}}\hat{\mathbf{z}}_1\\\hat{\mathbf{y}}\hat{\mathbf{x}}_1&\hat{\mathbf{y}}\hat{\mathbf{y}}_1&\hat{\mathbf{y}}\hat{\mathbf{z}}_1\\\hat{\mathbf{z}}\hat{\mathbf{x}}_1&\hat{\mathbf{z}}\hat{\mathbf{y}}_1&\hat{\mathbf{z}}\hat{\mathbf{z}}_1\end{pmatrix},\tag{83}$$

where $\hat{\mathbf{x}},\hat{\mathbf{y}},\hat{\mathbf{z}}$ and $\hat{\mathbf{x}}_1,\hat{\mathbf{y}}_1,\hat{\mathbf{z}}_1$ are the basis vectors of the coordinate systems $\{x,y,z\}$ and $\{x_1,y_1,z_1\}$, respectively.

If $|\mathbf{r}'|\gg|\mathbf{r}''|$, $k|\mathbf{r}'|\gg 1$ and $|\mathbf{r}''|\ll\sqrt{\lambda|\mathbf{r}'|}$, then the far-field zone approximation for the Green's function can be used:

$$\overleftrightarrow{G}_0(\mathbf{r}',\mathbf{r}'')=(\overleftrightarrow{I}-\hat{\mathbf{r}}'\otimes\hat{\mathbf{r}}')\frac{\exp(ik|\mathbf{r}'|)}{4\pi|\mathbf{r}'|}\exp(-ik\hat{\mathbf{r}}'\mathbf{r}'').\tag{84}$$

Appendix B. Scattering matrices definitions

Plane homogeneous electromagnetic wave has zero component along the direction of propagation given by the wave vector $\mathbf{k}$, so that the electric field $\mathbf{E}$ can be decomposed as follows:

$$\mathbf{E}=E_1\hat{\mathbf{x}}_1+E_2\hat{\mathbf{y}}_1,\tag{85}$$

where $\hat{\mathbf{x}}_1$ and $\hat{\mathbf{y}}_1$ are the basis vectors of the coordinate system $\{x_1,y_1,z_1\}$ with axis z_1 directed towards the wave vector $\mathbf{k}$ and with axis y_1 perpendicular to the meridional plane (i.e., the plane through the vector $\mathbf{k}$ and z-axis of the reference coordinate system $\{x,y,z\}$):

$$\frac{\mathbf{k}}{k}=\hat{\mathbf{x}}_1\times\hat{\mathbf{y}}_1,\quad \hat{\mathbf{y}}_1=\frac{\hat{\mathbf{z}}\times\mathbf{k}}{|\hat{\mathbf{z}}\times\mathbf{k}|}.\tag{86}$$

In the linear optics the component of the incident $(E_1^{inc},E_2^{inc})^T$ and scattered $(E_1^{sc},E_2^{sc})^T$ waves are related to each other by the amplitude scattering matrix $\mathbf{S}$ (see, for example, [35]):

$$\begin{pmatrix}E_1^{sc}\\E_2^{sc}\end{pmatrix}=\frac{e^{ikr}}{r}\mathbf{S}(\mathbf{n}_{sc},\mathbf{n}_{inc})\begin{pmatrix}E_1^{inc}\\E_2^{inc}\end{pmatrix},\tag{87}$$

$$\mathbf{S}(\mathbf{n}_{sc},\mathbf{n}_{inc})=\begin{pmatrix}S_{11}&S_{12}\\S_{21}&S_{22}\end{pmatrix},\tag{88}$$

where $\mathbf{n}_{inc}=\mathbf{k}_{inc}/k$, $\mathbf{n}_{sc}=\mathbf{k}_{sc}/k$, $\mathbf{k}_{inc}$ and $\mathbf{k}_{sc}$ are the wave vectors in the directions of incidence and scattering, respectively.

The Stokes parameters $(I,Q,U,V)^T$ are related to the components of electric fields (E_1,E_2) as follows (see, for example, [35]):

$$\begin{pmatrix}I\\Q\\U\\V\end{pmatrix}=\frac{1}{2}\sqrt{\frac{\varepsilon}{\mu}}\mathbf{D}\begin{pmatrix}|E_1|^2\\E_1E_2^*\\E_2^*E_1\\|E_2|^2\end{pmatrix},\tag{89}$$

$$\mathbf{D}=\begin{pmatrix}1&0&0&1\\1&0&0&-1\\0&-1&-1&0\\0&-i&i&0\end{pmatrix},\tag{90}$$

where ε is the complex electric permittivity and μ is the magnetic permeability of the medium.

The Stokes parameters of the incident and scattered radiations are related to each other by the phase matrix $\mathbf{Z}$ [35]:

$$\begin{pmatrix}I_{sc}\\Q_{sc}\\U_{sc}\\V_{sc}\end{pmatrix}=\frac{1}{r^2}\mathbf{Z}(\mathbf{n}_{sc},\mathbf{n}_{inc})\begin{pmatrix}I_{inc}\\Q_{inc}\\U_{inc}\\V_{inc}\end{pmatrix},\tag{91}$$

The elements of amplitude matrix $\mathbf{S}$ and phase matrix $\mathbf{Z}$ are related to each other [35]:

$$\mathbf{Z}(\mathbf{n}_{sc},\mathbf{n}_{inc})=\mathbf{D}\mathbf{Z}^J(\mathbf{n}_{sc},\mathbf{n}_{inc})\mathbf{D}^{-1},\tag{92}$$

$$\mathbf{Z}^J(\mathbf{n}_{sc},\mathbf{n}_{inc})=\begin{pmatrix}S_{11}S_{11}^*&S_{11}S_{12}^*&S_{12}S_{11}^*&S_{12}S_{12}^*\\S_{11}S_{21}^*&S_{11}S_{22}^*&S_{12}S_{21}^*&S_{12}S_{22}^*\\S_{21}S_{11}^*&S_{21}S_{12}^*&S_{22}S_{11}^*&S_{22}S_{12}^*\\S_{21}S_{21}^*&S_{21}S_{22}^*&S_{22}S_{21}^*&S_{22}S_{22}^*\end{pmatrix},\tag{93}$$

$$\mathbf{D}^{-1}=\frac{1}{2}\begin{pmatrix}1&1&0&0\\0&0&-1&i\\0&0&-1&-i\\1&-1&0&0\end{pmatrix}.\tag{94}$$

Fresnel phase matrix $\mathbf{Z}^{Fr}$ can be defined as follows:

$$\mathbf{Z}^{Fr}(m,\hat{\mathbf{r}},-\hat{\mathbf{r}}_0)=\mathbf{L}(\eta_v)\mathbf{M}^{Fr}(m,\gamma)\mathbf{L}(\eta_{inc}),\tag{95}$$

$$\mathbf{L}(\eta)=\begin{pmatrix}1&0&0&0\\0&\cos 2\eta&\sin 2\eta&0\\0&-\sin 2\eta&\cos 2\eta&0\\0&0&0&1\end{pmatrix},\tag{96}$$

$$\cos\eta_v=-\frac{\mu_0+\mu_v\cos\gamma}{\sqrt{1-\mu_v^2}\sin\gamma},\quad \sin\eta_v=\frac{\sqrt{1-\mu_0^2}\sin\phi}{\sin\gamma},\tag{97}$$

$$\cos\eta_{inc}=\frac{\mu_v+\mu_0\cos\gamma}{\sqrt{1-\mu_0^2}\sin\gamma},\quad \sin\eta_{inc}=\frac{\sqrt{1-\mu_v^2}\sin\phi}{\sin\gamma},\tag{98}$$

$$\mu_0=-\mathbf{n}_{inc}\hat{\mathbf{z}},\quad \mu_v=\mathbf{n}_{sc}\hat{\mathbf{z}},\tag{99}$$

$$\mathbf{M}^{Fr}(m,\gamma)=\frac{1}{2}\begin{pmatrix}|r_\parallel|^2+|r_\perp|^2&|r_\parallel|^2-|r_\perp|^2&0&0\\|r_\parallel|^2-|r_\perp|^2&|r_\parallel|^2+|r_\perp|^2&0&0\\0&0&r_\parallel r_\perp^*+r_\perp r_\parallel^*&-i(r_\parallel r_\perp^*-r_\perp r_\parallel^*)\\0&0&i(r_\parallel r_\perp^*-r_\perp r_\parallel^*)&r_\parallel r_\perp^*+r_\perp r_\parallel^*\end{pmatrix},\tag{100}$$

$$r_\parallel=\frac{m^2\mu_r-\sqrt{m^2-1+\mu_r^2}}{m^2\mu_r+\sqrt{m^2-1+\mu_r^2}},\tag{101}$$

$$r_\perp=\frac{\mu_r-\sqrt{m^2-1+\mu_r^2}}{\mu_r+\sqrt{m^2-1+\mu_r^2}},\tag{102}$$

$$\mu_r = \cos\theta_r, \quad \theta_r = (\pi - \gamma)/2, \quad \cos\gamma = (\mathbf{n}_{sc}\mathbf{n}_{inc}). \tag{103}$$

Here $\mathbf{M}^{Fr}$ is Fresnel reflection matrix, $\mathbf{L}(\eta_v)$ and $\mathbf{L}(\eta_{inc})$ are the Stokes rotation matrices for the angles η_v and η_{inc}; m is the complex refractive index of medium providing Fresnel reflection; $\phi = \varphi_{sc} - \varphi_{inc}$, φ_{sc}, φ_{inc} are azimuth angles of scattered and incident directions ($\mathbf{n}_{sc}$ and $\mathbf{n}_{inc}$).

References

[1] Tsang L, Kong JA, Shin RT. Theory of microwave remote sensing. New York: Wiley; 1985.
[2] Tsang L, Kong JA, Ding K-H. Scattering of electromagnetic waves: theories and applications. New York: Wiley; 2000.
[3] Tsang L, Kong JA, Ding K-H. Scattering of electromagnetic waves. Advanced topics. New York: Wiley; 2001.
[4] Mishchenko MI, Travis LD. Satellite retrieval of aerosol properties over the ocean using polarization as well as intensity of reflected sunlight. J Geophys Res 1997;102:16989–7013.
[5] Tanre D, Kaufman YJ, Herman M, Mattoo S. Remote sensing of aerosol properties over oceans using the MODIS/EOS spectral radiances. J Geophys Res 1997;102:16971–88.
[6] Chowdhary J, Cairns B, Mishchenko M, Hobbs P, Cota G, Redemann J, et al. Retrieval of aerosol scattering and absorption properties from photo-polarimetric observations over the ocean during the clams experiment. Atmos Sci 2005;62:1093–117.
[7] Hasekamp OP, Landgraf J. Retrieval of aerosol properties over the ocean from multispectral single-viewing angle measurements of intensity and polarization: retrieval approach, and sensitivity study. Geophys Res 2005;110:D20207.
[8] Hasekamp O, Litvinov P, Butz A. Aerosol properties over the ocean from PARASOL multi-angle photopolarimetric measurements. J Geophys Res 2011;116:D14204.
[9] Dubovik O, Herman M, Holdak A, Lapyonok T, Tanre D, Deuze JL, et al. Statistically optimized inversion algorithm for enhanced retrieval of aerosol properties from spectral multi-angle polarimetric satellite observations. Atmos Meas Technol 2011;4:975–1018.
[10] Roujean J-L, Leroy M, Deschamps P-Y. A bidiractional reflectance model of the Earth's surface for the correction of remote sensing data. J Geophys Res 1992;97(D18):20455–68.
[11] Wanner W, Li X, Strahlar AH. On the derivation of kernals for kernel-driven models of bidirectional reflectance. J Geophys Res 1995;100(D10):21077–89.
[12] Rahman H, Pinty B, Verstraete MM. Coupled Surface-Atmosphere Reflectance (CSAR) Model 2. Semiempirical surface model usable with NOAA advanced very high resolution radiometer data. J Geophys Res 1993;98(D11):20791–801.
[13] Spurr RJD. A new approach to the retrieval of surface properties from earthshine measurements. J Quant Spectrosc Radiat Transfer 2004;83:15–46.
[14] Rondeaux G, Herman M. Polarization of light reflected by crop canopies. Remote Sens Environ 1991;38:63–75.
[15] Knobelspiesse KD, Cairns B, Schaaf CB, Schmid B, Roman MO. Surface BDRF estimation from an aircraft compared to MODIS and ground estimates at the Southern Great Plains site. J Geophys Res 2008;113:D20105.
[16] Breon F-M, Tanre D, Lecomte P, Herman M. Polarized Reflectance of bare soil and vegetation: measurements and models. IEEE Trans Geosci Remote Sens 1995;33:487–99.
[17] Nadal F, Breon F-M. Parameterization of surface polarized reflectance derived from POLDER spaceborne measurements. IEEE Trans Geosci Remote Sens 1999;37:1709–18.
[18] Maignan F, Breon F-M, Fedele E, Bouvier M. Polarized reflectances of natural surfaces: spaceborne measurements and analytical modeling. Remote Sens Environ 2009;113:2642–50.
[19] Litvinov P, Hasekamp O, Cairns B. Models for surface reflection of radiance and polarized radiance: comparison with airborne multi-angle photopolarimetric measurements and implications for modeling top-of-atmosphere measurements. Remote Sens Environ 2011;115:781–92.
[20] Litvinov P, Hasekamp O, Cairns B, Mishchenko M. Semi-empirical BRDF and BPDF models applied to the problem of aerosol retrievals over land: testing an airborne data and implications for modeling of top-of-atmosphere measurements. In: Polarimetric detection, characterization, and remote sensing. Springer; 2011. p. 313–9.
[21] Deschamps PY, Breon FM, Leroy M, Podaire A, Bricaud A, Buriez JC, et al. The POLDER mission: instrument characteristics and scientific objectives. IEEE Trans Geosci Remote Sens 1994;32:598–615.
[22] Tanre D, Breon F-M, Deuze JL, Dubovik O, Ducos F, Francois F, et al. Remote sensing of aerosols by using polarized directional and spectral measurements within the A-Train: the PARASOL mission. Atmos Meas Technol 2011;4:1383–95.
[23] Bacour C, Breon F-M. Variability of biome reflectance directional signature as seen by POLDER. Remote Sens Environ 2005;98:80–95.
[24] Bacour C, Breon F-M, Maignan F. Normalisation of the directional effect on NOAA-AVHRR reflectances measurements for an improved monitoring of vegetation cycles. Remote Sens Environ 2006;102:402–13.
[25] Cairns B, Russel EE, Travis LD. The research scanning polarimeter: calibration and ground-based measurements. Proc SPIE 1999;3754:186.
[26] Elias T, Cairns B, Chowdhary J. Surface optical properties measured by the airborne research scanning polarimeter during the CLAMS experiment. Proc SPIE 2004;5235:595–606.
[27] Mishchenko M, Cairns B, Kopp G, Schueler G, Fafaul C, Hansen J, et al. Accurate monitoring of terrestrial aerosols and total solar irradiance: introducing the Glory mission. Bull Am Meteorol Soc 2007;88:677–91.
[28] Maignan F, Breon MF, Lacaze R. Bidirectional reflectance of Earth targets: evaluation of analytical models using a large set of spaceborne measurements with emphasis on the Hot Spot. Remote Sens Environ 2004;90:210–20.
[29] Muinonen K. Coherent backscattering of light by complex media of spherical scatterers: numerical solution. Wave Random Media 2004;14:365–88.
[30] Parviainen H, Muinonen K. Bidirectional reflectance of rough particulate media: ray-tracing solution. J Quant Spectrosc Radiat Transfer 2009;110:1418–40.
[31] Tishkovets VP, Jockers K. Multiple scattering of light by densely packed random media of spherical particles: dense media vector radiative transfer equation. J Quant Spectrosc Radiat Transfer 2006;101:54–72.
[32] Tishkovets VP, Petrova EV, Mishchenko MI. Scattering of electromagnetic waves by ensembles of particles and discrete random media. J Quant Spectrosc Radiat Transfer 2011;112:2095–127.
[33] Dlugach JM, Mishchenko MI, Liu L, Mackowski DW. Numerically exact computer simulations of light scattering by densely packed, random particulate media. J Quant Spectrosc Radiat Transfer 2011;112:2068–78.
[34] Mishchenko MI, Travis LD, Lacis AA. Multiple scattering of light by particles. Radiative transfer and coherent backscattering. Cambridge University Press; 2006.
[35] Mishchenko MI, Travis LD, Lacis AA. Scattering, absorption and emission of light by small particles. Cambridge University Press; 2002.
[36] Tsang L, Kong JA. Multiple scattering of electromagnetic waves by random distributions of discrete scatterers with coherent potential and quantum mechanical formalism. J Appl Phys 1980;51:3465–85.
[37] Litvinov P, Ziegler K. Rigorous derivation of superposition t-matrix approach from solution of inhomogeneous wave equation. J Quant Spectrosc Radiat Transfer 2008;109:74–8. http://dx.doi.org/10.1016/j.jqsrt.2007.07.001.
[38] Litvinov P. Derivation of extended boundary condition method from general definition of T-matrix elements and Lippman–Schwinger equation for transition operator. J Quant Spectrosc Radiat Transfer 2008;109:1440–6. http://dx.doi.org/10.1016/j.jqsrt.2007.11.001.
[39] Tsang L, Chen C, Chang ATC, Guo J, Ding K. Dense media radiative transfer theory based on quasicrystalline approximation with applications to passive microwave remote sensing of snow. Radio Sci 2000;35(N3):731–49.
[40] Varadan VK, Bringi VN, Varadan VV. Coherent electromagnetic wave propagation through randomly distributed dielectric scatters. Phys Rev D 1979;19(N8):2480–9.
[41] Mishchenlo MI, Dlugach JM. Coherent backscatter and the opposition effect for E-type asteroids. Planet Space Sci 1993;41:173–81.
[42] Mishchenko MI, Luck JM, Nieuwenhuizen ThM. Full angular profile of the coherent polarization affect. J Opt Soc Am A 2000;17:888–91.
[43] Tishkovets VP, Litvinov PV, Lyubchenko MI. Coherent opposition effects for semi-infinite discrete random medium in the double-scattering approximation. J Quant Spectrosc Radiat Transfer 2002;72:803–11.
[44] Litvinov P, Tishkovets V, Ziegler K. Coherent backscattering effects for discrete random media: numerical and theoretical results. J Quant Spectrosc Radiat Transfer 2007;103:131–45.

[45] Tishkovets VP, Mishchenko MI. Approximate calculation of coherent backscattering for semi-infinite discrete random media. J Quant Spectrosc Radiat Transfer 2009;110:139–45.
[46] Mishchenko MI. Directional radiometry and radiative transfer: a new paradigm. J Quant Spectrosc Radiat Transfer 2011;112: 2079–94.
[47] Schaepman-Strub G, Schaepman ME, Painter TH, Dangel S, Martonchik JV. Reflectance quantities in optical remote sensing – definitions and case studies. Remote Sens Environ 2006;103:27–42.
[48] Smith BG. Geometrical shadowing of a random rough surface. IEEE Trans Antennas Propag 1967;15:668–71.
[49] Sancer MI. Shadow-corrected electromagnetic scattering from a randomly rough surface. IEEE Trans Antennas Propag 1969;17: 577–85.
[50] Munoz O, Volten H, Hovenier JW, Nousiainen T, Muinonen K, Guirado D, et al. Scattering matrix of large Saharan dust particles: experiments and computations. J Geophys Res 2007;112:D13215.
[51] Tishkovets VP, Petrova EV, Jockers K. Optical properties of aggregate particles comparable in size to the wavelength. J Quant Spectrosc Radiat Transfer 2004;86:241–65.
[52] Dlugach JM, Mishchenko MI, Mackowski DW. Scattering and absorption properties of polydisperse wavelength-sized particles covered with much smaller grains. J Quant Spectrosc Radiat Transfer (2012), doi: http://dx.doi.org/10.1016/j.jqsrt.2012.03.006.
[53] Breon F-M, Fedele E, Maignan F, Lacaze R. A database of directional reflectance signature (GLC2000) with an analysis tool. A-Train Symposium, Lille; 22–25 October 2007.
[54] Litvinov P, Hasekamp O, Cairns B, Mishchenko M. Reflection models for soil and vegetation surfaces from multiple-viewing angle photopolarimetric measurements. J Quant Spectrosc Radiat Transfer 2010;111:529–39.
[55] Parviainen H, Muinonen K. Rough-surface shadowing of self-affine random rough surfaces. J Quant Spectrosc Radiat Transfer 2007;106: 398–416.